



Symmetric model of compressible granular mixtures with permeable interfaces

Richard Saurel, Sébastien Le Martelot, Robert Tosello, and Emmanuel Lapébie

Citation: Physics of Fluids (1994-present) **26**, 123304 (2014); doi: 10.1063/1.4903259

View online: <http://dx.doi.org/10.1063/1.4903259>

View Table of Contents: <http://scitation.aip.org/content/aip/journal/pof2/26/12?ver=pdfcov>

Published by the AIP Publishing

Articles you may be interested in

[Global Markov modelling and analysis of the dynamics of granular deformation and flow](#)
AIP Conf. Proc. **1542**, 563 (2013); 10.1063/1.4811993

[Simulations of granular bed erosion due to laminar shear flow near the critical Shields number](#)
Phys. Fluids **23**, 113303 (2011); 10.1063/1.3660258

[Simple Probabilistic Modeling of Granular Jamming and Validation Using DEM](#)
AIP Conf. Proc. **1145**, 507 (2009); 10.1063/1.3179973

[Effect of particle distribution on the compaction behavior of granular beds](#)
Phys. Fluids **18**, 066101 (2006); 10.1063/1.2213641

[Two-scale modeling in porous media: Relative permeability predictions](#)
Phys. Fluids **18**, 033101 (2006); 10.1063/1.2174877



Symmetric model of compressible granular mixtures with permeable interfaces

Richard Saurel,^{1,2} Sébastien Le Martelot,² Robert Tosello,³ and Emmanuel Lapébie⁴

¹*University Institute of France and Aix-Marseille University, CNRS IUSTI, 5 rue E. Fermi, 13453 Marseille Cedex 13, France*

²*RS2N, Chemin de Gaumin, 83640 Saint-Zacharie, France*

³*DGA-TN, 83050 Toulon, France*

⁴*CEA, DAM GRAMAT, F-46500 Gramat, France*

(Received 20 March 2014; accepted 15 November 2014; published online 15 December 2014)

Compressible granular materials are involved in many applications, some of them being related to energetic porous media. Gas permeation effects are important during their compaction stage, as well as their eventual chemical decomposition. Also, many situations involve porous media separated from pure fluids through two-phase interfaces. It is thus important to develop theoretical and numerical formulations to deal with granular materials in the presence of both two-phase interfaces and gas permeation effects. Similar topic was addressed for fluid mixtures and interfaces with the Discrete Equations Method (DEM) [R. Abgrall and R. Saurel, "Discrete equations for physical and numerical compressible multiphase mixtures," *J. Comput. Phys.* **186**(2), 361-396 (2003)] but it seemed impossible to extend this approach to granular media as intergranular stress [K. K. Kuo, V. Yang, and B. B. Moore, "Intragranular stress, particle-wall friction and speed of sound in granular propellant beds," *J. Ballist.* **4**(1), 697-730 (1980)] and associated configuration energy [J. B. Bdzil, R. Menikoff, S. F. Son, A. K. Kapila, and D. S. Stewart, "Two-phase modeling of deflagration-to-detonation transition in granular materials: A critical examination of modeling issues," *Phys. Fluids* **11**, 378 (1999)] were present with significant effects. An approach to deal with fluid-porous media interfaces was derived in Saurel *et al.* ["Modelling dynamic and irreversible powder compaction," *J. Fluid Mech.* **664**, 348-396 (2010)] but its validity was restricted to weak velocity disequilibrium only. Thanks to a deeper analysis, the DEM is successfully extended to granular media modelling in the present paper. It results in an enhanced version of the Baer and Nunziato ["A two-phase mixture theory for the deflagration-to-detonation transition (DDT) in reactive granular materials," *Int. J. Multiphase Flow* **12**(6), 861-889 (1986)] model as symmetry of the formulation is now preserved. Several computational examples are shown to validate and illustrate method's capabilities. © 2014 AIP Publishing LLC. [<http://dx.doi.org/10.1063/1.4903259>]

I. INTRODUCTION

Gas permeation effects in granular beds and through interfaces separating pure fluids and granular mixtures are present in many situations of interest, ranging from environmental considerations, with coastal erosion, for example, to the physics of highly energetic materials¹ as well as powder dissemination. The present work is related to this last category where many complex phenomena still need attention. Among them, powder compaction, shock propagation, deflagration to detonation transition, shock to detonation transition, fast deflagration are still challenging to model. Relevant contributions in these areas were done by many researchers and researcher groups over the world since the pioneer work of Andreev.²

The present contribution focuses on a fundamental issue related to the modelling and numerical approximation of granular mixture flows when the gas phase evolves with high speed, in the

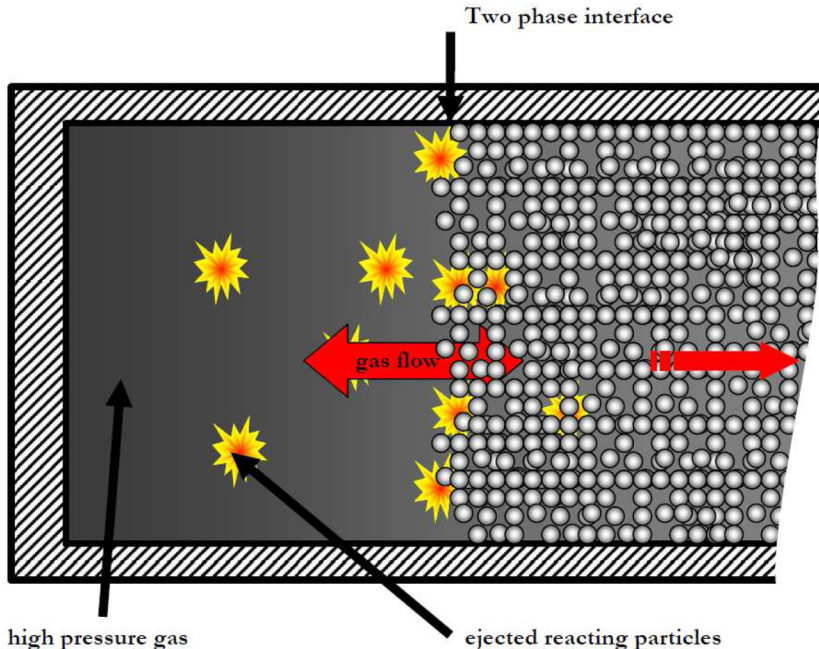


FIG. 1. Schematic representation of dense granular bed with packing effects, gas permeation, and two-phase interface. Grains are eventually carried off the interface by the gas flow when chemical decomposition occurs in the granular bed.

presence of shock and compaction waves as well as material interfaces separating gas zones and granular beds. A typical situation is schematized in Figure 1.

The introduction of granular effects (“configuration” pressure and related energy) in multiphase flow models has been addressed in Refs. 3 and 4. In former contributions to these references, granular effects were considered, but hyperbolicity of the equations was not guaranteed.^{5,6}

Theoretical formulations able to deal with both multiphase mixtures and material interfaces have been addressed in Refs. 7–9 to cite a few. In this last reference, an efficient approach to deal with non-conservative products (often called “nozzling terms” in the literature) was given through a discrete approach (the “Discrete Equations Method—DEM”). An important consequence rose with this formulation. Material interfaces separating fluids governed by different equations of state (EOSs) were solved routinely as well as non-equilibrium multiphase mixtures. Automatic fulfilment of equal normal velocities and equal pressures was obtained as soon as the volume fraction presented steep spatial evolutions. In zones of smooth volume fraction gradients, the two phases were evolving in full disequilibrium.

In the present work, we are looking for a flow model having the same features, but in the presence of granular effects. The Baer and Nunziato (BN)⁴ as well as Bdzil *et al.*³ formulations consider granular effects but are unable to consider material interfaces. To deal with material interfaces with multiphase flow formulations, two options are possible:

- Stiff relaxation methods, such as those detailed in Ref. 7. However, with stiff mechanical relaxation methods, gas permeation through interfaces is not possible.
- Non-conservative terms approach. This option has been considered in Ref. 1 considering quasi-steady nozzle flow through permeable interfaces. It has been considered by a different approach in Ref. 9 with the DEM. In this last option, there is no restriction regarding relative flow speed, presence of shocks, and materials’ equations of state. However, this approach has been developed for fluids only. It has been considered for turbulent flows in Ref. 10, reacting multiphase mixtures in Ref. 11, phase transition fronts and detonation waves in Ref. 12, and two-phase flows in ducts of variable cross section in Ref. 13. It is extended in the present work to granular mixtures in order to address gas permeation through interfaces.

In this aim, a fundamental difficulty appears. Indeed, the DEM is able to couple systems of hyperbolic equations, each system describing a pure phase having its thermodynamics governed by *phase* variables, such as phase density, phase internal energy or phase entropy, phase momentum, inner species concentrations, and so on. Here, configuration pressure and energy involve an *internal* variable to the *mixture* that is the volume fraction. This difficulty is addressed in the present paper.

The paper is organised as follows. In Sec. II, an “admissible system” of partial differential equations is examined. It has to be in agreement with the basic principles of physics such as the second law of thermodynamics. As wave propagation is of interest, the system must be hyperbolic. We also ask the equations to be *symmetric* in the sense that changes of material indexes should result in the same set of governing equations. This is not the case with existing granular models as the volume fraction is transported with the solid phase velocity and the pressure exerted on zones where volume fraction gradients are present (particle clouds boundaries) is assumed to be the gas pressure. We ask the flow model to have volume fraction transport velocity and interfacial pressure symmetric with respect to the phases. This feature is mandatory (at least) when dealing with material interfaces.¹⁰

In Sec. III, the DEM is developed for granular materials. The way the *internal mixture* variable (volume fraction) is considered in the formulation is detailed. The various Riemann solvers used in the DEM and in particular the granular one are summarized in the same section.

In Sec. IV, computed results are shown on basic examples, showing validity of the method. Comparison is done in the stiff mechanical relaxation limit with former results.¹⁴ Mechanical equilibrium flows are considered as well, showing perfect agreement and oscillation free solutions. Flows through permeable interfaces are then considered and qualitative comparisons are done in the presence and absence of granular effects.

Extension to extra physics is addressed in Sec. V with drag effects, heat transfers, and simplified modelling of granular combustion. Computational illustrations are shown in Sec. VI, with gradual insertion of the various physical effects. Conclusions and directions for future work are given in Sec. VII.

II. MODELLING GRANULAR MEDIA WITH GAS PERMEATION

Theoretical formulations of granular media examined hereafter are of Baer and Nunziato⁴ type. To model the effects of contacts and grains deformation, a “granular equation of state” is needed. It is presented hereafter before flow model examination.

A. Granular equation of state

Contrarily to fluids, granular media are subjected to grain contact effects. Rather than considering a complex 3D solid mechanics computational problem at the granular scale for each contact, their macroscopic effect is summarized in a granular EOS. The EOS parameters are determined from basic experiments of pressed powders. See Kuo *et al.*¹⁵ for a clear presentation of the experimental facility.

The granular pressure, denoted by β_1 in the following, is used to represent macroscopic effects of intergranular stress. The subscript 1 is used to denote the solid phase and the subscript 2 denotes the gas phase. The granular pressure β_1 is linked to the “granular energy” B_1 , representing the specific energy stored in the deformed layers around grains. In this frame, the total energy for the solid phase reads

$$E_1 = e_1(\rho_1, p_1) + B_1 + \frac{1}{2}u_1^2, \quad (2.1)$$

where e_1 , ρ_1 , and p_1 represent the internal energy, the density, and the pressure of the solid phase, respectively. u_1 represents the solid phase velocity and α_1 its volume fraction.

Following Ref. 3, the “granular energy,” B_1 is linked to the “granular pressure” through the following identity:

$$\beta_1 = \alpha_1 \rho_1 \frac{dB_1}{d\alpha_1}. \quad (2.2)$$

A similar identity was suggested in Ref. 4 with the solid Gibbs free energy instead of the energy B_1 .

The mechanical equilibrium among the solid and gas phases is reached when the phases have the same velocity and when the following identity is fulfilled:

$$\pi_1 = p_1 - \beta_1 = p_2 = \pi_2, \quad (2.3)$$

where π_k denote the phase k “effective” pressure.

It remains to give a formulation for the granular energy $B_1(\alpha_1)$. Following Ref. 14, the following function is appropriate:

$$B_1(\alpha_1) = \begin{cases} a \left((1 - \alpha_1) \ln(1 - \alpha_1) + (1 + \ln(1 - \alpha_1^0))(\alpha_1 - \alpha_1^0) - (1 - \alpha_1^0) \ln(1 - \alpha_1^0) \right)^n & \text{if } \alpha_1^0 < \alpha_1 < 1 \\ 0 & \text{otherwise} \end{cases}. \quad (2.4)$$

α_1^0 represents the threshold value from which the granular pressure and energy are non-zero. Parameters a , n , and α_1^0 are material dependant. Parameter “a” is a non-negative constant and “n” is a constant close to unity.

Using formulation (2.4) and granular pressure definition (2.2), computations have been done for granular HMX (cyclotetramethylene-tetrinitramine) with the following parameters: $\alpha_0 = 0.63$, $a = 3 \times 10^4$ Pa, and $n = 1.1$. In Figure 2, numerical results are shown in lines and compared to experimental data in bold lines, showing excellent agreement.

B. Admissible formulation of non-equilibrium granular media

To determine the flow model, a generic formulation is considered with various unknown parameters, θ , ϕ , P_1 , P'_1 , u_1 , and u'_1 . Parameters θ and ϕ can take 0 or 1 values only.

To select the correct model formulation, a list of criterion is considered:

- Second law of thermodynamics.
- Hyperbolicity.
- Symmetry of the formulation.
- Agreement with already known granular models in the absence of gas permeation.

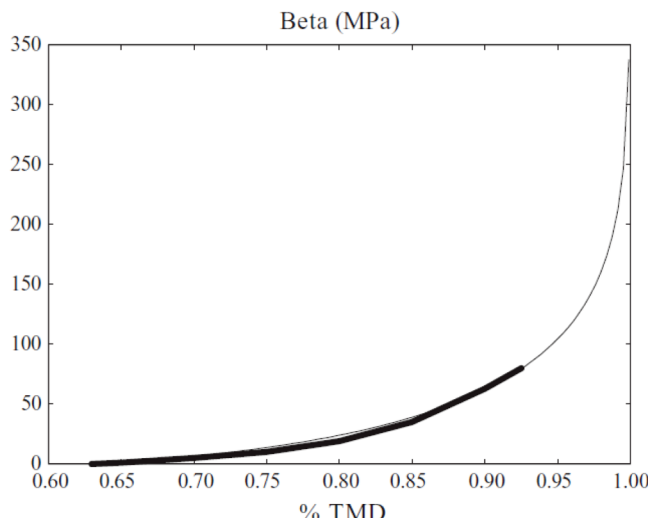


FIG. 2. Approximation of the experimental compression curve (bold lines) for granular HMX by the granular EOS (2.2–2.4) in lines. The fitting parameters are determined in the zone where the curves are superimposed, where the volume fraction ranges from 0.63 to 0.93. The percentage of theoretical maximum density is defined by %TMD = $(\alpha_1 \rho_1 / \rho_1^0)$.

The first two criterions are commonly accepted. The third one is the main new restriction the model has to fulfil.

The equations for phase 1 (solid phase) are presented hereafter, the formulation being symmetric for the second phase,

$$\begin{aligned} \frac{\partial \alpha_1}{\partial t} + u_1 \frac{\partial \alpha_1}{\partial x} &= \mu(\pi_1 - \pi_2), \\ \frac{\partial(\alpha\rho)_1}{\partial t} + \frac{\partial(\alpha\rho u)_1}{\partial x} &= 0, \\ \frac{\partial(\alpha\rho u)_1}{\partial t} + \frac{\partial(\alpha\rho u^2 + \alpha(p - \phi\beta))_1}{\partial x} &= P_1 \frac{\partial \alpha_1}{\partial x} + \lambda(u_2 - u_1), \\ \frac{\partial(\alpha\rho E)_1}{\partial t} + \frac{\partial(\alpha(\rho E + (p - \phi\beta))u)_1}{\partial x} &= P_1 u_1 \frac{\partial \alpha_1}{\partial x} + \lambda u'_1(u_2 - u_1) - \mu P'_1(\pi_1 - \pi_2) + Q_1. \end{aligned} \quad (2.5)$$

The phases total energies read $E_k = e_k + \theta B_k(\alpha_k, s_k) + \frac{1}{2} u_k^2$. (2.6)

The notations are conventional in two-phase flow literature. α , ρ , u , and p denote the volume fraction, the density, the velocity, and the pressure, respectively. λ and μ denote the velocity and pressure relaxation parameters, respectively. Q_1 denotes the convective heat exchange between the bulk temperature of phase 1 (T_1) and the interface. Q_1 is built so that $Q_1 + Q_2 = 0$. Details on the various exchange terms will be addressed in Sec. V. For the moment, we focus on terms that involve derivatives.

These terms involve interfacial variables, u_1 and u'_1 , P_1 and P'_1 . Their meaning is detailed in Ref. 10.

- u_1 and P_1 control the dynamics of particle clouds, as they express velocity transport and forces acting at volume fraction gradients (boundaries of granular clouds).
- u'_1 and P'_1 express the transport velocity and pressure acting at the particles surface inside the cloud of grains.

As shown in this reference and recalled later, these variables have been determined with the help of volume and surface averages of Riemann problem solutions.

Parameters θ and ϕ are introduced to re-examine modelling of these interfacial variables in the context of granular mixtures. Indeed, in total energy definition (2.6), Ref. 4 use $\theta = 0$ while Ref. 14 use $\theta = 1$. These authors considered $\phi = 0$. They also considered $u_1 = u'_1 = u_1$ (the solid phase velocity) and $P_1 = P'_1 = p_2$ (the gas phase pressure), while Ref. 10 considered symmetric formulas for these variables.

In definition (2.6), the granular energy is assumed to be dependent of the volume fraction, as done usually and the phase entropy s_k (obviously linked to the temperature). This option was not considered in Sec. II A (and previous authors) but we are interested in the following by the consequences of such dependency, as intuitively, granular pressure and energy seem temperature dependant.

To be more general, the granular energy could be considered as a function of two independent state variables of the considered phase, such as, for example, $B_k = B_k(\alpha_k, s_k, \rho_k)$. However, we assume that $B_k = B_k(\alpha_k, s_k)$ only as during powder compression experiments the granular pressure β_k is determined in a pressure range such that $\rho_k = \text{cst}$. When the material becomes compressible ($\rho_k \neq \text{cst}$), at elevated pressures, the related energy is included in the material equation of state $e_k = e_k(s_k, \rho_k)$.

The same argument could be used regarding the entropy dependency. However, it is rather clear that the same powder sample compressed at different initial temperatures behaves differently. We thus consider $B_k = B_k(\alpha_k, s_k)$.

Consequently, the granular pressure defined in Sec. II A now reads

$$\beta_k = \alpha_k \rho_k \left. \frac{\partial B_k}{\partial \alpha_k} \right|_{s_k}.$$

The configuration energy differential $B_k = B_k(\alpha_k, s_k)$ reads

$$dB_k = \frac{\beta_k}{\alpha_k \rho_k} d\alpha_k + \left. \frac{\partial B_k}{\partial s_k} \right|_{\alpha_k} ds_k.$$

Equipped with these definitions let us examine admissibility of formulation (2.5) with respect to the second law of thermodynamics. In this aim, System (2.5) is expressed in primitive variables ($\mathbf{W} = (\alpha_1, \rho_1, u_1, s_1)^T$) formulation,

$$\begin{aligned} \frac{d_1 \alpha_1}{dt} + (u_I - u_1) \frac{\partial \alpha_1}{\partial x} &= \mu(\pi_1 - \pi_2), \\ \alpha_1 \left(\frac{d_1 \rho_1}{dt} + \rho_1 \frac{\partial u_1}{\partial x} \right) &= \rho_1(u_I - u_1) \frac{\partial \alpha_1}{\partial x} - \rho_1 \mu(\pi_1 - \pi_2), \\ \frac{d_1 u_1}{dt} + \frac{1}{\rho_1} \frac{\partial p_1}{\partial x} - \phi \frac{1}{\rho_1} \frac{\partial \beta_1}{\partial x} &= \frac{(P_I - (p - \phi \beta_1))}{(\alpha \rho)_1} \frac{\partial \alpha_1}{\partial x} + \frac{\lambda}{(\alpha \rho)_1} (u_2 - u_1), \\ (\alpha \rho)_1 \left(T_1 + \theta \frac{\partial B_1}{\partial s_1} \right) \frac{d_1 s_1}{dt} &= \\ -\phi \frac{\alpha_1}{\rho_1} \beta_1 \frac{d_1 \rho_1}{dt} + (P_I - p_1 + (\theta + \phi) \beta_1)(u_I - u_1) \frac{\partial \alpha_1}{\partial x} & \\ + \lambda(u'_I - u_1)(u_2 - u_1) - \mu(P'_I - p_1 + (\theta + \phi) \beta_1)(\pi_1 - \pi_2) + Q_1. & \end{aligned} \quad (2.7)$$

The Lagrangian derivative along the phase 1 trajectory is denoted by $\frac{d_1}{dt} = \frac{\partial}{\partial t} + u_1 \frac{\partial}{\partial x}$.

A sufficient condition for the entropy inequality fulfilment is positivity of the right hand side of the entropy equation. As the sign of $\frac{d_1 \rho_1}{dt}$ is arbitrary, the parameter ϕ must be 0, in agreement with the aforementioned references.

Consequently, the momentum equation necessarily reads

$$\frac{\partial(\alpha \rho u)_1}{\partial t} + \frac{\partial(\alpha \rho u^2 + \alpha p)_1}{\partial x} = P_I \frac{\partial \alpha_1}{\partial x} + \lambda(u_2 - u_1).$$

The entropy equation becomes

$$\begin{aligned} (\alpha \rho)_1 \left(T_1 + \theta \frac{\partial B_1}{\partial s_1} \right) \frac{d_1 s_1}{dt} &= (P_I - (p_1 - \theta \beta_1))(u_I - u_1) \frac{\partial \alpha_1}{\partial x} \\ + \lambda(u'_I - u_1)(u_2 - u_1) - \mu(P'_I - (p_1 - \theta \beta_1))(\pi_1 - \pi_2) + Q_1. & \end{aligned}$$

Two options are now considered.

$$\bullet \quad \theta = 0$$

In that instance, the entropy equation becomes

$$(\alpha \rho)_1 T_1 \frac{d_1 s_1}{dt} = (P_I - p_1)(u_I - u_1) \frac{\partial \alpha_1}{\partial x} + \lambda(u'_I - u_1)(u_2 - u_1) + \mu(p_1 - P'_I)(\pi_1 - \pi_2) + Q_1.$$

Following Ref. 10, velocity and interfacial pressures can be expressed from Riemann problem solution,

$$\begin{aligned} u_I &= u'_I + \text{sgn} \left(\frac{\partial \alpha_1}{\partial x} \right) \frac{p_2 - p_1}{Z_1 + Z_2}, \\ u'_I &= \frac{Z_1 u_1 + Z_2 u_2}{Z_1 + Z_2}, \\ P_I &= P'_I + \text{sgn} \left(\frac{\partial \alpha_1}{\partial x} \right) \frac{Z_1 Z_2}{Z_1 + Z_2} (u_2 - u_1), \\ P'_I &= \frac{Z_2 p_1 + Z_1 p_2}{Z_1 + Z_2}, \end{aligned} \quad (2.8)$$

where $Z_k = \rho_k c_k$ represents the acoustic impedance of the phase k .

A difficulty appears for the last term: $\mu(p_1 - P'_I)(\pi_1 - \pi_2)$.

If the interfacial pressure is taken as $P'_I = p_2 + \beta_1$, the last term for phase 1 reads $\mu(\pi_1 - \pi_2)^2$.

But for the second phase, the entropy production term is not necessarily positive, $\mu(p_2 - P'_I)(\pi_2 - \pi_1) = \mu\beta_1(\pi_1 - p_2)$. This drawback was corrected by³ taking $\theta = 1$ in the solid phase energy definition.

Consequently, when the option $\theta = 0$ is used, granular effects must be absent of the equations. For instance, the volume fraction equation must read

$$\frac{\partial \alpha_1}{\partial t} + u_I \frac{\partial \alpha_1}{\partial x} = \mu(p_1 - p_2)$$

instead of

$$\frac{\partial \alpha_1}{\partial t} + u_I \frac{\partial \alpha_1}{\partial x} = \mu(\pi_1 - \pi_2).$$

With closure relations (2.8), the symmetric two-fluid model of Ref. 10 is thus recovered. We now consider the last option with $\theta = 0$.

$$\bullet \quad \theta = 1$$

The entropy equation now reads

$$(\alpha\rho)_I \left(T_I + \frac{\partial B_I}{\partial s_I} \right)_{\alpha_1} \frac{d_I s_I}{dt} = (P_I - \pi_1)(u_I - u_1) \frac{\partial \alpha_1}{\partial x} + \lambda(u'_I - u_1)(u_2 - u_1) - \mu(P'_I - \pi_1)(\pi_1 - \pi_2) + Q_1.$$

The following interfacial variables' estimates satisfy systematically the second law of thermodynamics and preserve symmetry of the formulation:

$$\begin{aligned} u_I &= \frac{Z_1 u_1 + Z_2 u_2}{Z_1 + Z_2} + \text{sgn}\left(\frac{\partial \alpha_1}{\partial x}\right) \frac{\pi_2 - \pi_1}{Z_1 + Z_2}, \\ u'_I &= \frac{Z_1 u_1 + Z_2 u_2}{Z_1 + Z_2}, \\ P_I &= \frac{Z_2 \pi_1 + Z_1 \pi_2}{Z_1 + Z_2} + \text{sgn}\left(\frac{\partial \alpha_1}{\partial x}\right) \frac{Z_1 Z_2}{Z_1 + Z_2} (u_2 - u_1), \\ P'_I &= \frac{Z_2 \pi_1 + Z_1 \pi_2}{Z_1 + Z_2}. \end{aligned} \quad (2.9)$$

The positive function $\frac{\partial B_I}{\partial s_I} \Big|_{\alpha_1}$ expresses the temperature dependence to compaction effects. This function has never been determined in the author's knowledge. Experiments should be done in this direction, as intuitively, compaction effects are dependant on the solid temperature.

The only admissible flow model with regard to the second law of thermodynamics and symmetry of the formulation is thus given in Sec. II C. The granular energy dependence $\frac{\partial B_I}{\partial s_I} \Big|_{\alpha_1}$ is removed due to the lack of experimental knowledge.

C. Granular flow model

The two-phase flow model that results of the former analysis reads

phase 1:

$$\begin{aligned} \frac{\partial \alpha_1}{\partial t} + u_I \frac{\partial \alpha_1}{\partial x} &= \mu(\pi_1 - \pi_2), \\ \frac{\partial(\alpha\rho)_I}{\partial t} + \frac{\partial(\alpha\rho u)_I}{\partial x} &= 0, \\ \frac{\partial(\alpha\rho u)_I}{\partial t} + \frac{\partial(\alpha\rho u^2 + \alpha p)_I}{\partial x} &= \pi_1 \frac{\partial \alpha_1}{\partial x} + \lambda(u_2 - u_1), \\ \frac{\partial(\alpha\rho E)_I}{\partial t} + \frac{\partial(\alpha(\rho E + p)u)_I}{\partial x} &= \pi_1 u_I \frac{\partial \alpha_1}{\partial x} + \lambda u'_I (u_2 - u_1) - \mu \pi'_I (\pi_1 - \pi_2) + Q_1; \end{aligned}$$

phase 2:

$$\begin{aligned} \frac{\partial(\alpha\rho)_2}{\partial t} + \frac{\partial(\alpha\rho u)_2}{\partial x} &= 0, \\ \frac{\partial(\alpha\rho u)_2}{\partial t} + \frac{\partial(\alpha\rho u^2 + \alpha p)_2}{\partial x} &= \pi_1 \frac{\partial \alpha_2}{\partial x} - \lambda(u_2 - u_1), \\ \frac{\partial(\alpha\rho E)_2}{\partial t} + \frac{\partial(\alpha(\rho E + p)u)_2}{\partial x} &= \pi_1 u_1 \frac{\partial \alpha_2}{\partial x} - \lambda u'_1(u_2 - u_1) + \mu \pi'_1 (\pi_1 - \pi_2) + Q_2. \end{aligned} \quad (2.10)$$

With the following definitions:

- The phases total energies read $E_k = e_k + B_k(\alpha_k) + \frac{1}{2}u_k^2$.
- The granular pressure is defined by $\beta_k = \alpha_k \rho_k \frac{dB_k}{d\alpha_k}$.
- The interfacial variables read

$$\begin{aligned} u_I &= \frac{Z_1 u_1 + Z_2 u_2}{Z_1 + Z_2} + \operatorname{sgn}\left(\frac{\partial \alpha_1}{\partial x}\right) \frac{\pi_2 - \pi_1}{Z_1 + Z_2}, \\ u'_I &= \frac{Z_1 u_1 + Z_2 u_2}{Z_1 + Z_2}, \\ \pi_I &= \frac{Z_2 \pi_1 + Z_1 \pi_2}{Z_1 + Z_2} + \operatorname{sgn}\left(\frac{\partial \alpha_1}{\partial x}\right) \frac{Z_1 Z_2}{Z_1 + Z_2} (u_2 - u_1), \\ \pi'_I &= \frac{Z_2 \pi_1 + Z_1 \pi_2}{Z_1 + Z_2}. \end{aligned}$$

The notation P_I has been replaced by π_I as the interfacial pressure involves effective pressures $\pi_k = p_k - \beta_k$.

This symmetric formulation of the BN model has some advantages. To be precise, with the original BN-type models, two options are possible with interfacial variables:

- $P_I = p_g$ (gas pressure) and $u_I = u_s$ (solid velocity). This is the BN original choice, in agreement with the second law of thermodynamics.
- $P_I = p_s$ (solid pressure) and $u_I = u_g$ (gas velocity). This choice is also in agreement with the second law of thermodynamics.

These two options result in different computed results. There are thus arbitrary choices with these variables when both materials are compressible and at high density, such as in situations involving shocks and detonations in condensed energetic materials. With symmetric formulations, this drawback disappears and the two former options appear as limit cases when $Z_1 \gg Z_2$ or $Z_2 \gg Z_1$.

Another important consequence is that these symmetric interfacial variables are local “granular Riemann problem” solutions that enable handling of fluid-granular interfaces as well as permeable interfaces as will be shown in Secs. III and IV.

Moreover, System (2.10) has the following mixture entropy equation:

$$\begin{aligned} \frac{\partial(\alpha\rho)_1 s_1 + (\alpha\rho)_2 s_2}{\partial t} + \frac{\partial(\alpha\rho)_1 u_1 s_1 + (\alpha\rho)_2 u_2 s_2}{\partial x} &= \frac{Q_1}{T_1} + \frac{Q_2}{T_1} \\ \frac{1}{T_1} \left\{ \frac{Z_1}{(Z_1 + Z_2)^2} \left((\pi_2 - \pi_1) + \operatorname{sgn}\left(\frac{\partial \alpha_1}{\partial x}\right) Z_2 (u_2 - u_1) \right)^2 \left| \frac{\partial \alpha_1}{\partial x} \right| + \lambda \frac{Z_2}{Z_1 + Z_2} (u_2 - u_1)^2 + \mu \frac{Z_1}{Z_1 + Z_2} (\pi_2 - \pi_1)^2 \right\} \\ + \frac{1}{T_2} \left\{ \frac{Z_2}{(Z_1 + Z_2)^2} \left((\pi_2 - \pi_1) + \operatorname{sgn}\left(\frac{\partial \alpha_1}{\partial x}\right) Z_2 (u_2 - u_1) \right)^2 \left| \frac{\partial \alpha_2}{\partial x} \right| + \lambda \frac{Z_1}{Z_1 + Z_2} (u_2 - u_1)^2 + \mu \frac{Z_2}{Z_1 + Z_2} (\pi_2 - \pi_1)^2 \right\}. \end{aligned}$$

As $Q_1 + Q_2 = 0$ and as will be shown latter Q_1 is proportional to $(T_2 - T_1)$, all production terms appearing in this equation are non-negative.

This flow model is clearly symmetric in the sense that interchange of the material indexes results in the same set of governing equations, having thus no consequence on the results.

We now address the last remaining tests, regarding hyperbolicity of the equations and agreement with already known model of granular media.

1. Hyperbolicity

System hyperbolicity is now addressed. The system expressed in primitive variables (2.7) is considered in the absence of relaxation terms. It reads

$$\frac{\partial \mathbf{W}}{\partial x} + \mathbf{A}(\mathbf{W}) \frac{\partial \mathbf{W}}{\partial x} = 0, \quad (2.11)$$

with

$$\mathbf{A}(\mathbf{W}) = \begin{pmatrix} u_I & 0 & 0 & 0 \\ -\frac{\rho_1}{\alpha_1}(u_I - u_1) & u_1 & \rho_1 & 0 \\ -\frac{(\pi_I - p_1)}{(\alpha\rho)_1} & \frac{c_1^2}{\rho_1} & u_1 & \frac{1}{\rho_1} \frac{\partial p_1}{\partial s_1} \\ -\frac{(\pi_I - p_1)(u_I - u_1)}{(\alpha\rho)_1 T_1} & 0 & 0 & u_1 \end{pmatrix}.$$

The associated wave speeds are $\lambda_1 = u_I$, $\lambda_1 = u_1$, $\lambda_2 = u_1 + c_1$, and $\lambda_3 = u_1 - c_1$. Similar wave speeds are obtained for the second phase. As expected, the system is hyperbolic.

2. Mechanical equilibrium asymptotic limit

The asymptotic analysis follows the lines of Ref. 8. Each flow variable f is assumed to obey the expansion $f = f^0 + \epsilon f^1$, where f^0 represents the mechanical equilibrium state and f^1 a small perturbation around it. Oppositely, mechanical relaxation parameters are supposed stiff $\lambda = \epsilon^{-1}$, $\mu = \epsilon^{-1}$.

To obtain the volume fraction equation, it is sufficient to examine the two pressure evolution equations. In the limit of stiff velocity relaxation, they become at leading order

$$\begin{aligned} \alpha_1 \left(\frac{dp_1}{dt} + \rho_1 c_1^2 \frac{\partial u}{\partial x} \right) &= -\mu (\Gamma_1(\pi'_I - \pi_1) + \rho_1 c_1^2) (\pi_1 - \pi_2) + \Gamma_1 Q_1, \\ \alpha_2 \left(\frac{dp_2}{dt} + \rho_2 c_2^2 \frac{\partial u_2}{\partial x} \right) &= \mu (\Gamma_2(\pi'_I - \pi_2) + \rho_2 c_2^2) (\pi_1 - \pi_2) + \Gamma_2 Q_2, \end{aligned}$$

where Γ_k is the Gruneisen coefficient of phase k , and the Lagrangian derivative now reduces to

$$\frac{d}{dt} = \frac{\partial}{\partial t} + u \frac{\partial}{\partial x}.$$

These equations have to be complemented by granular pressure contributions. The granular pressure definition corresponds to Eq. (2.2). Differentiating this equation along a trajectory yields

$$\frac{d\beta_k}{dt} = \alpha_k \rho_k \frac{d^2 B_k}{d\alpha_k^2} \frac{d\alpha_k}{dt} - \alpha_k \rho_k \frac{dB_k}{d\alpha_k} \frac{\partial u}{\partial x}.$$

For phase 1 in the presence of stiff velocity relaxation, the volume fraction equation reads

$$\frac{d\alpha_1}{dt} = \mu(\pi_1 - \pi_2).$$

The corresponding granular pressure equation thus reads

$$\frac{d\beta_1}{dt} + \beta_1 \frac{\partial u}{\partial x} = \alpha_1 \rho_1 \frac{d^2 B_1}{d\alpha_1^2} \mu(\pi_1 - \pi_2).$$

We now add this equation to the thermodynamic pressure evolution equation for phase 1

$$\frac{d(p_1 - \beta_1)}{dt} + (\rho_1 c_1^2 - \beta_1) \frac{\partial u}{\partial x} = \frac{-\mu (\Gamma_1(\pi'_I - \pi_1) + \rho_1 C_1^2) (\pi_1 - \pi_2) + \Gamma_1 Q_1}{\alpha_1}.$$

Considering stiff pressure relaxation, this equation reduces to

$$\frac{d(p_1 - \beta_1)}{dt} + (\rho_1 c_1^2 - \beta_1) \frac{\partial u}{\partial x} = -\frac{\rho_1 C_1^2}{\alpha_1} (\pi_1^I - \pi_2^I) + \frac{\Gamma_1 Q_1}{\alpha_1}.$$

Obviously, for phase 2 it reads

$$\frac{d(p_2 - \beta_2)}{dt} + (\rho_2 c_2^2 - \beta_2) \frac{\partial u}{\partial x} = \frac{\rho_2 C_2^2}{\alpha_2} (\pi_1^1 - \pi_2^1) + \frac{\Gamma_2 Q_2}{\alpha_2},$$

with $C_k^2 = c_k^2 + \alpha_k^2 \frac{d^2 B_k}{da_k^2}$.

Taking the difference of these two equations, the time derivative stress vanishes and the stress fluctuation difference is obtained as

$$\pi_1^1 - \pi_2^1 = \frac{((\rho_2 c_2^2 - \beta_2) - (\rho_1 c_1^2 - \beta_1)) \partial u}{\frac{\rho_1 C_1^2}{\alpha_1} + \frac{\rho_2 C_2^2}{\alpha_2}} + Q_1 \frac{\frac{\Gamma_1}{\alpha_1} + \frac{\Gamma_2}{\alpha_2}}{\frac{\rho_1 C_1^2}{\alpha_1} + \frac{\rho_2 C_2^2}{\alpha_2}}.$$

Inserting this relation into the volume fraction equation for phase 1 in the presence of stiff velocity and pressure relaxation,

$$\frac{da_1}{dt} = (\pi_1^1 - \pi_2^1),$$

the mechanical equilibrium model of Kapila *et al.*⁸ is recovered,

$$\begin{aligned} \frac{da_1}{dt} &= \frac{((\rho_2 c_2^2 - \beta_2) - (\rho_1 c_1^2 - \beta_1)) \partial u}{\frac{\rho_1 C_1^2}{\alpha_1} + \frac{\rho_2 C_2^2}{\alpha_2}} + Q_1 \frac{\alpha_2 \Gamma_1 + \alpha_1 \Gamma_2}{\alpha_2 \rho_1 C_1^2 + \alpha_1 \rho_2 C_2^2}, \\ \frac{\partial(\alpha \rho)_1}{\partial t} + \frac{\partial(\alpha \rho)_1 u}{\partial x} &= 0, \\ \frac{\partial(\alpha \rho)_2}{\partial t} + \frac{\partial(\alpha \rho)_2 u}{\partial x} &= 0, \\ \frac{\partial \rho u}{\partial t} + \frac{\partial \rho u^2 + p}{\partial x} &= 0, \\ \frac{\partial \rho E}{\partial t} + \frac{\partial(\rho E + p)u}{\partial x} &= 0, \end{aligned}$$

with

$$E = Y_1(e_1(\rho_1, p_1) + B_1(\alpha_1)) + Y_2(e_2(\rho_2, p_2) + B_2(\alpha_2)) + \frac{1}{2} u^2.$$

The non-equilibrium model is thus in agreement with the limit model of Ref. 8.

III. THE DISCRETE EQUATIONS METHOD FOR GRANULAR MEDIA

We now address derivation of the DEM to determine the discrete analogue of System (2.10). This method is of particular interest for the reasons that follow.

The conventional way to proceed is to build the two-phase flow model with some appropriate method (time and space averaging method, kinetic-type method, Hamilton-principle method, or the thermodynamic method considered in Sec. II) resulting in a set of partial differential equations. Then, it is conventional to address difference theory of hyperbolic systems to build a numerical scheme. In the frame of non-conservative hyperbolic equations, such a theory is absent. Indeed, discontinuous waves are present, and flow functions may become discontinuous. For example, P_1 may become a Heaviside function. Also, the same flow may involve volume fraction discontinuities (two-phase interfaces). In this context, the volume fraction is a Heaviside function too and its derivative is a Dirac function. The product of a Dirac and Heaviside function is undefined. This is why conventional methods fail with two-phase interfaces and conventional theory for the building of numerical schemes fails. This was explained in detail in Ref. 9. Heaviside functions associated to shock existence in two-phase media appear at least when relaxation effects among the phases are

weak. When they are stiff, shocks become disperse^{16,17} and when they are arbitrary, several types of shock profiles are possible, involving discontinuities.

To overcome the difficulties related to non-conservative products, a fine scale description of the thin zone where volume fraction has stiff variation is needed. Schwendeman *et al.*¹⁸ suggested a nozzle flow type solution where both stagnation enthalpy and entropy are constant in this layer. We prefer the method given in Ref. 9 as it is not restricted to isentropic quasi-steady flows. It is based on a micro-scale description addressed at the discrete level.

The method proceeds in a non-conventional way in the sense that interface problems (Riemann problem solutions) for pure material equations (Euler equations for fluids, more sophisticated models for other media) are averaged on a two-phase computational cell giving a discrete Godunov-type scheme. The issue of Heaviside and Dirac functions product is solved as, at the subcell scale, wave diffraction occurs at the scale of each discontinuity of the phases' presence function. The physical wave diffraction process results in a locally constant pressure that is multiplied without ambiguity by the Dirac function. This diffraction process is schematized in Figure 3.

From these discrete equations (actually a two-phase numerical scheme), it is possible to determine the set of partial differential equations that are solved. In the context of two fluids mixtures, it corresponds to the system given in Ref. 10 where symmetric closure relations appear for the interfacial variables as well as an extra wave speed. As shown in the present (and former) paper, these slight differences compared to the BN model have importance.

However, from this "theory" based on discrete equations and continuous limit, it seemed impossible to insert granular effects. This is solved in the present section, thanks to the structure of the granular model derived previously (2.10).

We first recall the DEM basis in the case of two fluids mixtures and address granular effects second.

A. Two fluids version

Each phase is compressible and governed by the Euler equations. In order to take into account the two-phase flow topology, these equations are considered in two dimensions

$$\frac{\partial \mathbf{U}}{\partial t} + \frac{\partial \mathbf{F}}{\partial x} + \frac{\partial \mathbf{G}}{\partial y} = 0 \quad (3.1)$$

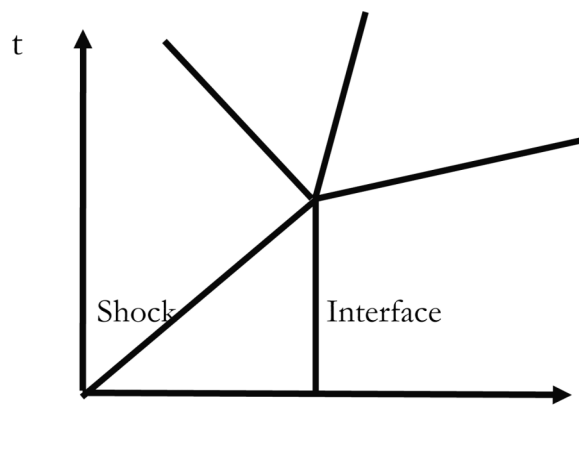


FIG. 3. Schematic representation of a shock-material interface interaction. The interface is initially at rest and the shock is right facing. The shock wave diffraction results in transmitted and reflected waves. At the interface location, the pressure and velocity are continuous before and after shock interaction, rendering unambiguous product of these functions with the presence function gradient that corresponds to a Dirac function.

with

$$\mathbf{U} = \begin{pmatrix} 1 \\ \rho \\ \rho u \\ \rho v \\ \rho E \end{pmatrix}, \quad \mathbf{F} = \begin{pmatrix} 0 \\ \rho u \\ \rho u^2 + p \\ \rho uv \\ (\rho E + p) u \end{pmatrix}, \text{ and } \mathbf{G} = \begin{pmatrix} 0 \\ \rho v \\ \rho uv \\ \rho v^2 + p \\ (\rho E + p) v \end{pmatrix},$$

where \mathbf{U} represents the conservative variable vector, \mathbf{F} and \mathbf{G} represent the associated flux vectors in the x and y directions, ρ represents the density (kg m^{-3}), u represents the x -velocity component (m s^{-1}), v represents the y -velocity component (m s^{-1}), E represents the total energy (J/kg), and p represents the pressure (Pa).

Adding the equation $\frac{\partial 1}{\partial t} + \frac{\partial \rho}{\partial x} + \frac{\partial \rho}{\partial y} = 0$ is convenient to determine the volume fraction equation.

In order to take into account the interactions between the two phases, and therefore obtain the equations associated to each phase in the two-phase mixture, the Euler equations are multiplied by the characteristic function $X_k(M, t)$, where M denotes a point in space, and t denotes the time. Thus, $X_k(M, t) = 1$ if the point M is located inside the k phase at time t and $X_k(M, t) = 0$ otherwise.

This function obeys the evolution equation,

$$\frac{\partial X_k}{\partial t} + \sigma_x \frac{\partial X_k}{\partial x} + \sigma_y \frac{\partial X_k}{\partial y} = 0, \quad (3.2)$$

where σ_x and σ_y denote the local interface velocity components.

Multiplying Euler equations (3.1) by the characteristic function gives

$$X_k \frac{\partial \mathbf{U}}{\partial t} + X_k \frac{\partial \mathbf{F}}{\partial x} + X_k \frac{\partial \mathbf{G}}{\partial y} = 0$$

which can be re-written as

$$\frac{\partial X_k \mathbf{U}}{\partial t} + \frac{\partial X_k \mathbf{F}}{\partial x} + \frac{\partial X_k \mathbf{G}}{\partial y} = F^{\text{lag}} \frac{\partial X_k}{\partial x} + G^{\text{lag}} \frac{\partial X_k}{\partial y}, \quad (3.3)$$

where $F^{\text{lag}} = (\mathbf{F} - \sigma_x \mathbf{U})$ and $G^{\text{lag}} = (\mathbf{G} - \sigma_y \mathbf{U})$ represent the Lagrangian fluxes (or “Hugoniot” fluxes when $\vec{\sigma} \neq \vec{u}$). In the frame of fluid mixtures without reaction fronts and phase transition, the interface velocity is equal to the fluid velocity at the interface. Therefore, $\sigma_x = u$ and $\sigma_y = v$. This leads to the following Lagrangian flux vectors:

$$F^{\text{lag}} = (-u, 0, p, 0, pu)^T \text{ and } G^{\text{lag}} = (-v, 0, p, 0, pv)^T.$$

Contrarily to conventional numerical methods, here the products

$$F^{\text{lag}} \frac{\partial X_k}{\partial x} \text{ and } G^{\text{lag}} \frac{\partial X_k}{\partial y}$$

are always well defined as shown in Figure 3. The shock diffraction process is accounted for in the Riemann problems considered hereafter. Its solution always results in constant pressure and constant normal velocity across the interface, that corresponds precisely to the location where X_k is discontinuous. Non-conservative products become unambiguous.

Equation (3.3) now needs to be integrated over the two-phase control volume that corresponds to a computational cell in the frame of the DEM.

B. Numerical integration

In this part, the space and time integration of System (3.3) is considered

$$\int_0^{\Delta t} \int_{C_i} \left(\frac{\partial X_k \mathbf{U}}{\partial t} + \frac{\partial X_k \mathbf{F}}{\partial x} + \frac{\partial X_k \mathbf{G}}{\partial y} \right) dV dt = \int_0^{\Delta t} \int_{C_i} \left(F^{\text{lag}} \frac{\partial X_k}{\partial x} + G^{\text{lag}} \frac{\partial X_k}{\partial y} \right) dV dt, \quad (3.4)$$

where C_i denotes a computational cell.

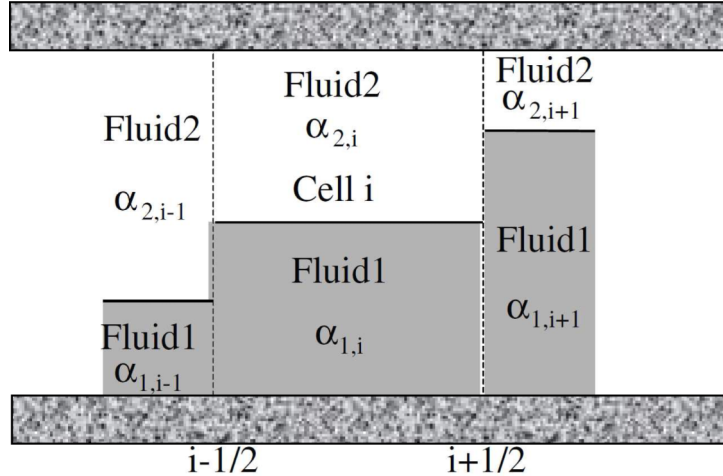


FIG. 4. Reference stratified two-phase flow topology. The i cell is connected to two cells, $i - 1$ and $i + 1$, through the cell boundaries, $i - 1/2$ and $i + 1/2$.

To proceed in these integrals' calculation, a 2D flow topology has to be specified. It has been shown in Chinnayya *et al.*¹¹ that stratified and bubbly flow topologies were yielding the same results for the fluxes and non-conservative terms discrete formulas. The relaxation terms only were different, but they are not under focus at present. For the sake of simplicity in the calculations, stratified two-phase flow topology is thus considered, as shown in Figure 4.

Each cell C_i has a volume V_i and is bounded by $i - 1/2$ and $i + 1/2$ cell edges. At each cell boundary, 4 types of contacts are possible between the left fluid $l \in \{1, 2\}$ and the right fluid $m \in \{1, 2\}$: “1-1,” “2-1,” “2-2,” and “1-2.” To each of these contacts (lm) are associated contact lengths L_{lm} , Eulerian fluxes F_{lm}^* , Lagrangian fluxes $F_{lm}^{lag,*}$, and values of the characteristic function X_{lm}^* as well as its associated jump $[X^*]_{lm}$. For the $i - 1/2$ cell boundary, the corresponding functions are given in Tables I and II.

TABLE I. Elements to compute the Eulerian flux integral for phase 1 at cell boundary $i - 1/2$.

Contact	Contact length	Eulerian flux	Characteristic function X_1^*
1-1	$L_{11,i-1/2} = \Delta y \text{Min}(\alpha_{1,i-1}, \alpha_{1,i})$	$F_{11,i-1/2}^*$	$X_{1,11,i-1/2}^* = 1$
1-2	$L_{12,i-1/2} = \Delta y \text{Max}(0, \alpha_{1,i-1} - \alpha_{1,i})$	$F_{12,i-1/2}^*$	$X_{1,12,i-1/2}^* = \begin{cases} 1 & \text{if } u_{12}^* > 0 \\ 0 & \text{if } u_{12}^* < 0 \end{cases}$
2-1	$L_{21,i-1/2} = \Delta y \text{Max}(0, \alpha_{1,i} - \alpha_{1,i-1})$	$F_{21,i-1/2}^*$	$X_{1,21,i-1/2}^* = \begin{cases} 1 & \text{if } u_{21}^* < 0 \\ 0 & \text{if } u_{21}^* > 0 \end{cases}$
2-2	$L_{22,i-1/2} = \Delta y \text{Min}(\alpha_{2,i-1}, \alpha_{2,i})$	$F_{22,i-1/2}^*$	$X_{1,22,i-1/2}^* = 0$

TABLE II. Elements to compute the Lagrangian flux integral for phase 1 at cell boundary $i - 1/2$.

Contact	Contact length	Lagrangian flux	Jump $[X_1^*]$
1-1	$L_{11,i-1/2}$	$F_{11,i-1/2}^{lag,*}$	$[X_1^*]_{11,i-1/2} = 0$
1-2	$L_{12,i-1/2}$	$F_{12,i-1/2}^{lag,*}$	$[X_1^*]_{12,i-1/2} = \begin{cases} -1 & \text{if } u_{12}^* > 0 \\ 0 & \text{if } u_{12}^* < 0 \end{cases}$
2-1	$L_{21,i-1/2}$	$F_{21,i-1/2}^{lag,*}$	$[X_1^*]_{21,i-1/2} = \begin{cases} 1 & \text{if } u_{21}^* > 0 \\ 0 & \text{if } u_{21}^* < 0 \end{cases}$
2-2	$L_{22,i-1/2}$	$F_{22,i-1/2}^{lag,*}$	$[X_1^*]_{22,i-1/2} = 0$

The volume fraction $\alpha_{k,i}$ has a simple link with the characteristic function

$$\alpha_{k,i} \stackrel{\text{def}}{=} \frac{V_{k,i}}{V_i} = \frac{1}{V_i} \int_{C_i} X_k dV.$$

With this definition and with the help of Tables I and II, the space-time integration of (3.4) gives the following numerical scheme that is precisely the DEM:

$$\frac{(a_k \{U_k\})_i^{n+1} - (a_k \{U_k\})_i^n}{\Delta t} + \frac{\sum_{l,m} (IX_k^* F^*)_{lm,i+1/2} - \sum_{l,m} (IX_k^* F^*)_{lm,i-1/2}}{\Delta x} = \frac{\sum_{l,m} (I[X_k^*] F^{lag,*})_{lm,i-1/2} + \sum_{l,m} (I[X_k^*] F^{lag,*})_{lm,i+1/2}}{\Delta x}. \quad (3.5)$$

Δx represents the space step in the x direction, Δt represents the numerical time step, and $l_{lm} = \frac{L_{lm}}{\Delta y}$ represent the cross section length ratios, where Δy represents the duct height considered in Figure 4.

The aim is to determine the volume fraction α_k and the set of average conservative variables $\{U_k\}$ at time t^{n+1} . To do this, the Eulerian and Lagrangian flux vectors F_{lm}^* and $F_{lm}^{lag,*}$ for each contact and each cell boundary ($i - 1/2$ and $i + 1/2$) have to be computed. Riemann solvers are considered in this aim. The difference between fluid and granular mixtures appears at this level.

C. Riemann solvers for fluids and granular mixtures

The various Eulerian and Lagrangian fluxes that appear in Tables I and II are obtained from the Riemann problem solution for the *Euler* equations. This is a very attractive point of the DEM as it solves two-phase flows with single phase Riemann solvers.

When dealing with fluid mixtures, users' favourite Riemann solvers can be used such as, for example,

- the Harten-Lax-van Leer-Contact (HLLC, Toro *et al.*¹⁹),
- the exact Riemann solver (Godunov²⁰),
- the “acoustic” Riemann solver (Toro²¹).

The DEM has been developed with these solvers in Refs. 10–12.

When dealing with granular mixtures, a fundamental difficulty appears. If a solver for the Euler equations is considered, the continuous limit of discrete formula (3.5) will not correspond to continuous model (2.10) derived previously. Calculation details of the continuous limit are given in Ref. 10. For example, the momentum equation for phase 1 will read

$$\frac{\partial(\alpha\rho u)_1}{\partial t} + \frac{\partial(\alpha\rho u^2 + \alpha p)_1}{\partial x} = p_1 \frac{\partial\alpha_1}{\partial x} + \lambda(u_2 - u_1)$$

instead of

$$\frac{\partial(\alpha\rho u)_1}{\partial t} + \frac{\partial(\alpha\rho u^2 + \alpha p)_1}{\partial x} = \pi_1 \frac{\partial\alpha_1}{\partial x} + \lambda(u_2 - u_1).$$

To be in agreement with continuous model (2.10), fluid type Riemann solver has to be considered in the Eulerian fluxes computation and “granular” Riemann solver has to be considered in the Lagrangian ones.

Let us detail these two kinds of solvers in the context of the HLLC solver, as it is both robust and accurate.

1. Fluid-fluid Riemann solver

This solver is detailed in Refs. 19 and 21. The wave diagram associated to the Riemann problem between two pure fluids is the same as in the single phase flow context, as shown in Figure 5. There are three waves denoted by S_L , S_R , and S_M , separating the states (L and R) located on each side of the contact discontinuity.

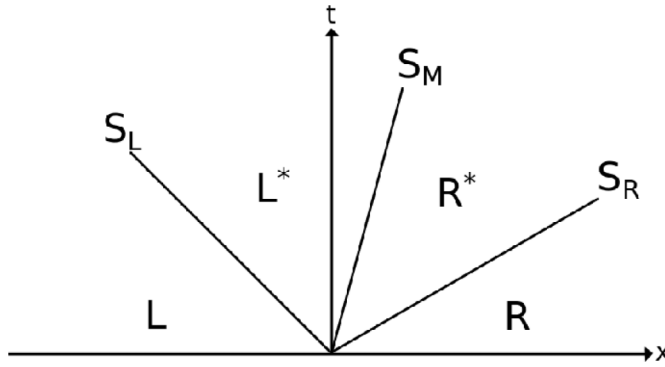


FIG. 5. Wave diagram associated to the Riemann problem with two fluids governed by the Euler equations.

S_L and S_R are computed using the Davis estimates:

$$\begin{aligned} S_L &= \min(u_L - c_L, u_R - c_R), \\ S_R &= \min(u_L + c_L, u_R + c_R), \end{aligned} \quad (3.6)$$

where u_L and c_L represent the phase velocity and the sound speed in the left state L , respectively, while u_R and c_R represent the same variables in the right state R . The intermediate wave speed S_M is determined under HLL approximation (Toro²¹),

$$S_M = \frac{p_R - p_L + \rho_R u_R (u_R - S_R) - \rho_L u_L (u_L - S_L)}{\rho_L (S_L - u_L) - \rho_R (S_R - u_R)}. \quad (3.7)$$

Now that the three waves S_L , S_R , and S_M are estimated, the Rankine-Hugoniot jump relations are used through S_L and S_R ,

$$\begin{aligned} F_L - S_L U_L &= F_L^* - S_L U_L^*, \\ F_R - S_R U_R &= F_R^* - S_R U_R^*, \end{aligned} \quad (3.8)$$

where $U = \begin{pmatrix} \rho \\ \rho u \\ \rho E \end{pmatrix}$ and $F = \begin{pmatrix} \rho u \\ \rho u^2 + p \\ (\rho E + p)u \end{pmatrix}$.

The following * states are obtained as

$$p^* = p_L + \rho_L (u_L - S_M) (u_L - S_L) = p_R + \rho_R (u_R - S_M) (u_R - S_R),$$

i.e.,

$$p^* = \frac{1}{2} [p_L + p_R + \rho_L (u_L - S_M) (u_L - S_L) + \rho_R (u_R - S_M) (u_R - S_R)]$$

and

$$\begin{aligned} \rho_{L*} &= \frac{\rho_L (u_L - S_L)}{S_M - S_L}, & \rho_{R*} &= \frac{\rho_R (u_R - S_R)}{S_M - S_R}, \\ E_{L*} &= \frac{\rho_L E_L (u_L - S_L) + p_L u_L - S_M p^*}{\rho_L (u_L - S_L)}, & E_{R*} &= \frac{\rho_R E_R (u_R - S_R) + p_R u_R - S_M p^*}{\rho_R (u_R - S_R)}. \end{aligned} \quad (3.9)$$

The solution state U^* used to determine the Eulerian solution flux F^* is determined using the following sampling:

$$\begin{aligned} &\text{If } S_L > 0, U^* = U_L. \\ &\text{If } S_R < 0, U^* = U_R. \\ &\text{If } S_L < 0, S_R > 0, \text{ and } S_M > 0, U^* = U_L^* \\ &\text{otherwise } U^* = U_R^*. \end{aligned} \quad (3.10)$$

The Lagrangian flux F^{lag} is determined using S_M and p^* : $F^{\text{lag}} = (-S_M, 0, p^*, 0, p^* S_M)^T$.

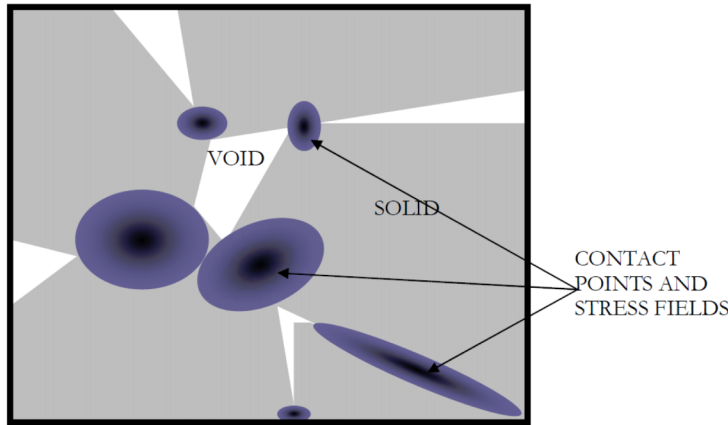


FIG. 6. Schematic representation of some contacts between grains and stress fields around them.

2. Granular Riemann solver

When dealing with a Riemann problem with a fluid and a granular media or two granular media in contact, the determination of S_M and the Eulerian flux calculations are unchanged.

The main change comes from the contact condition that now reads

$$\pi_L^* = \pi_R^*. \quad (3.11)$$

Indeed, when two granular media are in contact, the interface condition corresponds to normal equal velocities and equal normal stresses resulting in (3.11). A granular media can be schematized as shown in Figure 6.

Far from contacts, solids are considered as compressible materials governed by the Euler equations. Close to contacts only, solid materials behave as elastic-plastic media. The sum of these contacts is summarized in the configuration pressure β_{solid} . Thus, for a contact surface separating two packed granular beds, condition (3.11) replaces the pressure equilibrium condition. It also holds for an interface separating a fluid and a granular bed.

To obtain a symmetric relation, let us consider that the left and right states are granular media

$$\pi^* = p_L^* - \beta_L^* = p_R^* - \beta_R^*.$$

We now examine insertion of this contact interface condition in the HLLC solver.

The Rankine-Hugoniot momentum equation of the left facing wave for a given phase reads

$$p_L + \rho_L u_L (u_L - S_L) = p_L^* + \rho_L^* S_M (S_M - S_L).$$

This relation is unchanged compared to fluids as the materials far from the interfaces are governed by the Euler equations. It can also be written as

$$p_L - \beta_L^* + \rho_L u_L (u_L - S_L) = p_L^* - \beta_L^* + \rho_L^* S_M (S_M - S_L),$$

where the same granular pressure β_L^* has been added to both sides of the equation. It becomes

$$\pi_L + (\beta_L - \beta_L^*) + \rho_L u_L (u_L - S_L) = \pi^* + \rho_L^* S_M (S_M - S_L).$$

Similarly, the relation for the R side reads

$$\pi_R + (\beta_R - \beta_R^*) + \rho_R u_R (u_R - S_R) = \pi^* + \rho_R^* S_M (S_M - S_R).$$

Therefore, summing these two relations and extracting π^* , we obtain

$$\pi^* = \frac{1}{2} \{ \pi_L + \pi_R + (\beta_L - \beta_L^*) + (\beta_R - \beta_R^*) + \rho_L (u_L - S_L) (u_L - S_M) + \rho_R (u_R - S_R) (u_R - S_M) \}.$$

With the help of (3.9),

$$\beta_L^* = \alpha_L \rho_L^* \frac{dB}{d\alpha}(\alpha_L) = \alpha_L \rho_L \frac{u_L - S_L}{S_M - S_L} \frac{dB}{d\alpha}(\alpha_L) = \beta_L \frac{u_L - S_L}{S_M - S_L}.$$

Thus,

$$\pi^* = \frac{1}{2} \left\{ \pi_L + \pi_R + \beta_L \frac{S_M - u_L}{S_M - S_L} + \beta_R \frac{S_M - u_R}{S_M - S_R} + \rho_L (u_L - S_L) (u_L - S_M) + \rho_R (u_R - S_R) (u_R - S_M) \right\}.$$

Consequently, the Lagrangian flux is computed as

$$F^{lag} = (-S_M, 0, \pi^*, 0, \pi^* S_M)^T.$$

The Eulerian flux is still given by relations (3.7), (3.9), and (3.10). To be precise, the fluid-fluid HLLC Riemann solver is used to compute Eulerian flux, while the granular HLLC solver is used to compute the contact granular stress and associated Lagrangian flux.

D. The tricky point

When dealing with the DEM, the first ingredient consists in setting the single phase equations governing a given phase. These equations must form a system of conservation laws,

$$\frac{\partial U}{\partial t} + \frac{\partial F}{\partial x} = 0.$$

Second, selecting the appropriate equations for a given phase by the characteristic function X_k , the following result is obtained

$$\frac{\partial X_k U}{\partial t} + \frac{\partial X_k F}{\partial x} = F^{lag} \frac{\partial X_k}{\partial x},$$

where $F^{lag} = (F - u_i U)$ denotes the Lagrangian flux and u_i denotes the local interface velocity.

When the Euler equations are considered, the Lagrangian flux reads

$$F^{lag} = (-u, 0, p, pu)^T.$$

Thus, setting the system of conservation laws constrains the Lagrangian flux and consequently the non-conservative terms.

In Secs. III A–III C, the Euler equations have been used in the phases, but the non-conservative terms involve the pressure π instead of the thermodynamic pressure “p.” There is thus a contradiction.

This contraction disappears as soon as Figure 6 is well understood. Far from the interfaces, the Euler equations are valid in each material. Close to the interfaces, boundary layers’ effects appear, related to the presence of elastic and plastic effects. Their integration results in a local contact interface condition different of pressure equality and obviously results in different average contact conditions. Rather than considering this complicated boundary layer problem, it is sufficient to adopt the physically correct contact condition (here, Eq. (3.11)).

Mathematically, it means that F^{lag} is not necessarily equal to $(F - u_i U)$ when U and F are related to *far field* equations (here the Euler equations). F^{lag} is equal to $(F - u_i U)$ when U and F are related to the system of partial differential equations valid in the vicinity of the interface. Here, it should be an elastic-plastic model such as given, for example, in Gavrilyuk *et al.*²² But there is no interest to consider such complexity. Therefore, there is no contraction in using the Euler equations in each pure material as far field equations and have Lagrangian flux such that

$$F^{lag} \neq (F - u_i U)_{\text{Far field equations}}. \quad (3.12)$$

The identity

$$F^{lag} = (F - u_i U)_{\text{Local equations}}$$

is still valid with the equations valid at the interface.

E. Continuous limit of the discrete equations

A last verification is due. It is necessary to check that discrete Eq. (3.5) (that corresponds to a numerical scheme) tends to the continuous system of partial differential Eq. (2.10) when both time

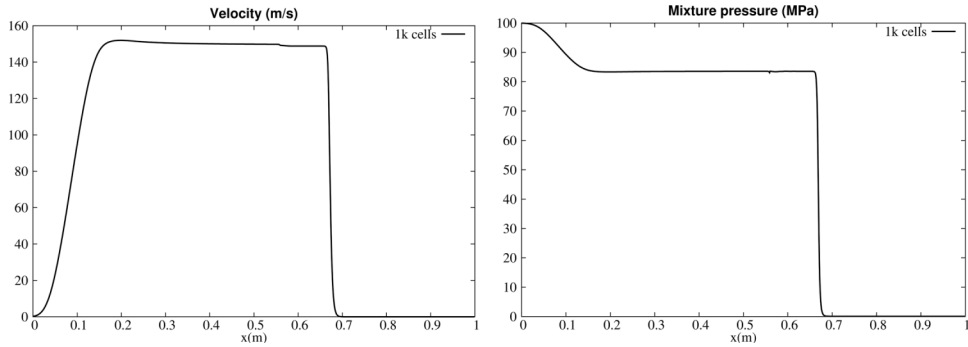


FIG. 7. Computed mixture velocity and pressure ($\alpha_1 p_1 + \alpha_2 p_2$) at time $t = 0.38$ ms resulting of the present non-equilibrium model combined with stiff mechanical relaxation solvers.

and space steps tend to zero. Such analysis has been carried out in Ref. 10 in the context of a fluid mixture model. In the present paper, granular effects are present.

Let us consider the temporal term of Eq. (3.5). When the space step Δx tends to zero, the conservative variables cell average $\{U_k\}$ tends to U_k . Consequently,

$$\frac{(\alpha_k \{U_k\})_i^{n+1} - (\alpha_k \{U_k\})_i^n}{\Delta t} \xrightarrow[\Delta t \rightarrow 0]{\Delta x \rightarrow 0} \frac{\partial \alpha_k U_k}{\partial t}, \quad (3.13)$$

with $U_k = (1, \rho_k, \rho_k u_k, \rho_k v_k, \rho_k E_k)^T$.

As shown in Ref. 10, the velocity component v_k vanishes if the flow topology is symmetric, such as annular flows (see Figure 7 of that reference) or presenting many inclusions, such as granular mixtures. Thanks to this remark, (3.13) corresponds to the temporal term of System (2.10).

The two-phase flux for a given phase k in (3.5) is obtained as a composite sum of the Euler equations fluxes as $\sum_{l,m} (I X_k^* F^*)_{lm}$.

In this composite flux, the Euler flux F_{lm}^* for the contact pair (lm) is always sampled in the considered phase k . Moreover, the indicator function $X_{k,lm}^*$ is non-zero only if the phase k is crossing the cell boundary. Also, l_{lm} is a surface fraction at the cell boundary that tends to the volume fraction, when the space step tends to zero. Last, the Euler flux F_{lm}^* is computed with the fluid-fluid Riemann solver detailed in Sec. III C, implying that the pressure p is present in both momentum and energy equations. Consequently, the flux difference appearing in (3.5) tends to

$$\frac{\sum_{l,m} (I X_k^* F^*)_{lm,i+1/2} - \sum_{l,m} (I X_k^* F^*)_{lm,i-1/2}}{\Delta x} \xrightarrow[\Delta x \rightarrow 0]{} \frac{\partial \alpha_k F_k}{\partial x}, \quad (3.14)$$

where $F_k = (0, \rho_k u_k, \rho_k u_k^2 + p_k, \rho_k u_k v_k, (\rho_k E_k + p_k) u_k)^T$ represents the flux of the Euler equations. Therefore, (3.14) corresponds to the flux derivatives appearing in System (2.10).

It remains to examine the Lagrangian flux sum appearing in the right-hand side of (3.5),

$$\frac{\sum_{l,m} (I [X_k^*] F^{lag,*})_{lm,i-1/2} + \sum_{l,m} (I [X_k^*] F^{lag,*})_{lm,i+1/2}}{\Delta x}.$$

To do this, the same calculations as in Ref. 10 (pp. 304-306) are done, resulting in

- $-u_l \frac{\partial \alpha_k}{\partial x}$, for the first component of this vector;
- 0, for the second component, as the mass equation that has zero Lagrangian flux;
- $\pi_l \frac{\partial \alpha_k}{\partial x}$, for the third component;
- 0, for the fourth component, as the mixture topology is considered symmetric, resulting in vanishing pressure integral and;
- $\pi_l u_l \frac{\partial \alpha_k}{\partial x}$, for the fifth component.

In these formulas, u_I and π_I are deduced from the acoustic analogue of the “granular Riemann solver” given in Sec. III C. To derive acoustic relations from the Rankine-Hugoniot conditions used in this section, there is just to replace the wave speeds S_L by $u_L - c_L$ and S_R by $u_R - c_R$. This approximation is valid in the continuous limit calculations context, where the flow functions are continuous. The interfacial velocity and pressure appearing in the non-conservative terms consequently read

$$u_I = \frac{Z_1 u_1 + Z_2 u_2}{Z_1 + Z_2} + \operatorname{sgn}\left(\frac{\partial \alpha_1}{\partial x}\right) \frac{\pi_2 - \pi_1}{Z_1 + Z_2} \text{ and}$$

$$\pi_I = \frac{Z_2 \pi_1 + Z_1 \pi_2}{Z_1 + Z_2} + \operatorname{sgn}\left(\frac{\partial \alpha_1}{\partial x}\right) \frac{Z_1 Z_2}{Z_1 + Z_2} (u_2 - u_1).$$

This is a key point of the present method. If the fluid-fluid Riemann solver is used instead of the “granular one” the discrete equations tend to a two-fluid mixture model instead of the granular two-phase model (2.10).

To conclude, when the fluid-fluid Riemann solver is used for the Eulerian flux (3.14) computation and the granular one for the Lagrangian flux computation, discrete Eq. (3.5) tends to continuous model (2.10) when both time and space steps tend to zero.

IV. COMPUTED RESULTS

To check validity of the preceding model and associated algorithms, we consider a test problem involving a fluid–granular media interface. Computations have been done in Ref. 14 with a mechanical equilibrium model, i.e., involving a single velocity and a single mechanical stress. To make comparisons, both stiff velocity and stress relaxation solvers have to be used with the present non-equilibrium model. Details regarding such solvers are given in Appendix A.

A. Powder compaction

We consider a 1 m long “shock tube” involving a high pressure chamber on the left, filled with gas at the initial pressure of 0.1 GPa and a low pressure chamber on the right, filled with granular HMX and air. The gas is governed by the ideal gas EOS with air polytropic coefficient while the granular material is governed by the stiffened-gas EOS. The different parameters are shown in Table III.

The configuration energy parameters for the HMX are $\alpha_0 = 0.63$, $a = 3 \times 10^4$ J, and $n = 1.1$.

An initial volume fraction discontinuity is present in the tube at abscissa 0.5 m. In order to prevent division by zero in the flow model, the solid volume fraction in the left chamber is set to 10^{-6} while in the right chamber, it is set to 0.63. The initial density of solid is constant in the whole domain and equal to 1903 kg/m^3 . Similarly, the gas phase density is constant in the whole domain and equal to 100 kg/m^3 . Both initial states are initially at rest.

Results are shown in Figure 7 at time 0.38 ms while the results obtained by Ref. 14 are shown in Figure 8. Both computations involve 1000 cells.

The results obtained by the present method are in good agreement with the ones obtained in Ref. 14. Nevertheless, some discrepancies appear at the interface, possibly due to the relaxation splitting. To check method’s convergence, the same computation is rerun with meshes involving 2000 cells and 4000 cells. Close up view of the results are shown in Figure 9.

TABLE III. EOS parameters of the materials under interest.

	$\rho_0 (\text{kg/m}^3)$	γ	$p_\infty (\text{Pa})$
HMX	1903	5.5	31×10^8
Air	1	1.4	0

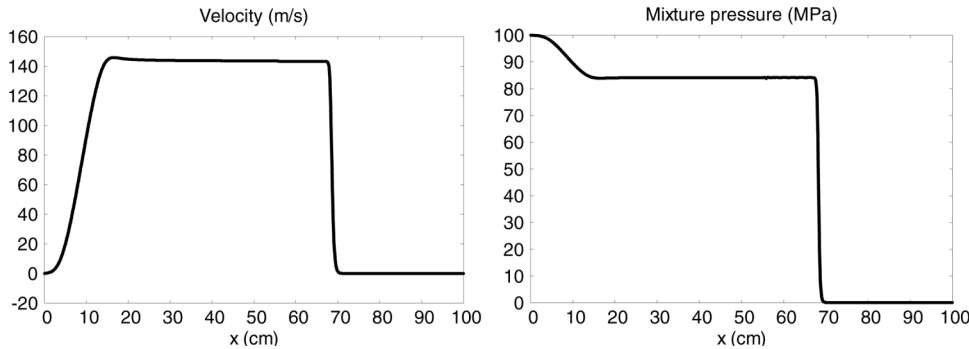


FIG. 8. Computed mixture velocity and pressure ($\alpha_1 p_1 + \alpha_2 p_2$) at time $t = 0.38$ ms obtained with the mechanical equilibrium model of Ref. 14.

These results show that the interface conditions mismatch is not relevant and is vanishing with mesh refinement. Therefore, the method converges to the solution given in Ref. 14.

It is interesting to report the zones where the configuration energy and corresponding granular pressure are non-zero. As expected, they are in compacted zones, as shown by the volume fraction graph shown in Figure 10.

B. Gas permeation

We now consider a “shock tube” of 0.7 m length involving a high pressure (30 MPa) and high temperature (1000 K) gas chamber on the left of and a low pressure (1 atm) and low temperature (293 K) chamber on the right, filled with the same granular mixture as in the first test case. As we are going gradually to consider combustion effects, the gas is expected to reach high densities and the Noble-Abel EOS is more appropriate than the ideal gas EOS. The solid material is still governed by the stiffened-gas EOS with the parameters given in Table III. Details regarding the Noble-Abel EOS are given in Appendix B. The gas covolume is taken as $\eta = 0.0003 \text{ m}^3/\text{kg}$, the specific heat at constant volume is taken as $C_v = 5000 \text{ J kg}^{-1} \text{ K}^{-1}$ and the specific heat ratio is unchanged ($\gamma = 1.4$). Obviously, it is possible to consider more sophisticated EOS (see for example Ref. 11), but this is not the aim of this presentation.

An initial volume fraction discontinuity is thus present in the tube at abscissa 0.2. The solid volume fraction in the left chamber is set to 10^{-6} ; in the right chamber, it is set to 0.63. Both initial states are initially at rest. Computed results are shown at time 0.05 ms and 0.1 ms. The mesh contains 1000 cells.

In order to have reference solutions in the absence of granular effects, a first run is made with the two fluids model. The results are shown in Figure 11.

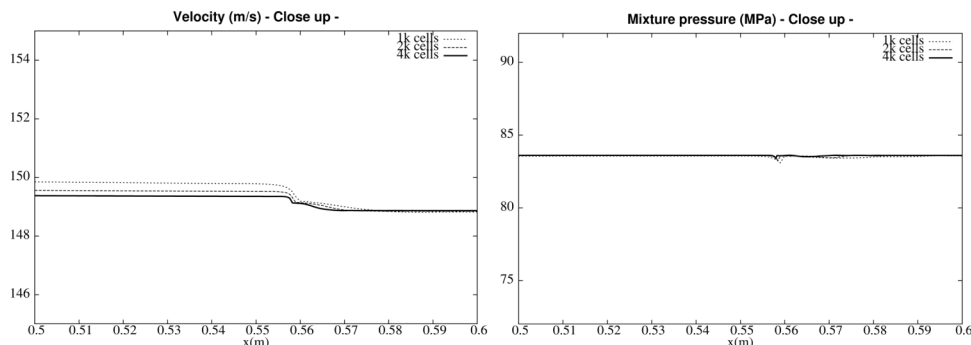


FIG. 9. Close up view of mixture velocity and pressure profiles near the interface at time $t = 0.38$ ms for several meshes (1000 cells, 2000 cells, and 4000 cells).

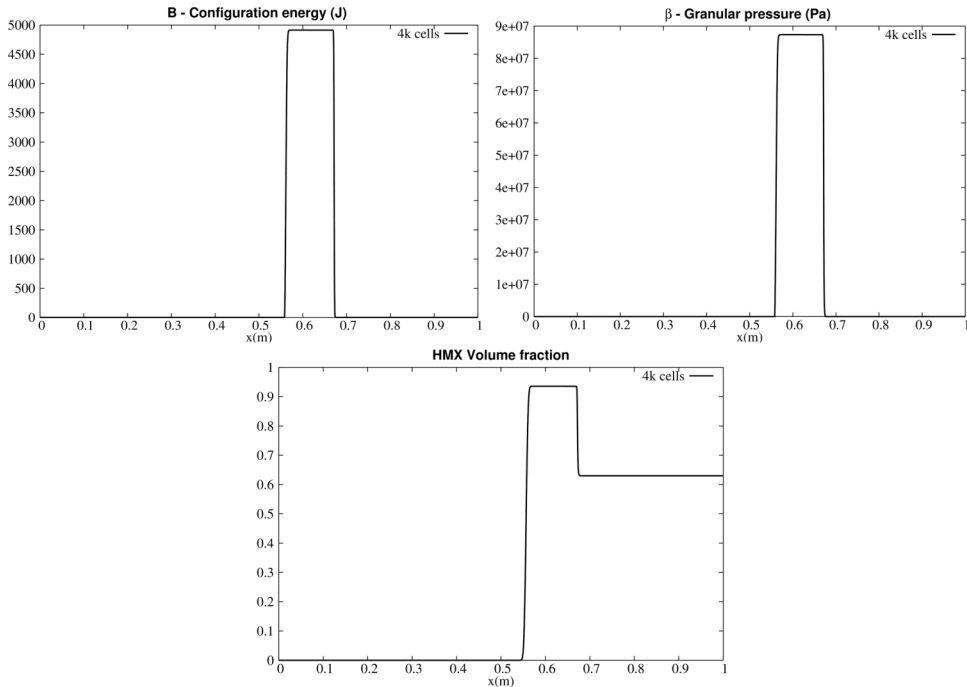


FIG. 10. Configuration energy, granular pressure, and HMX volume fraction at time $t = 0.38$ ms (4000 cells).

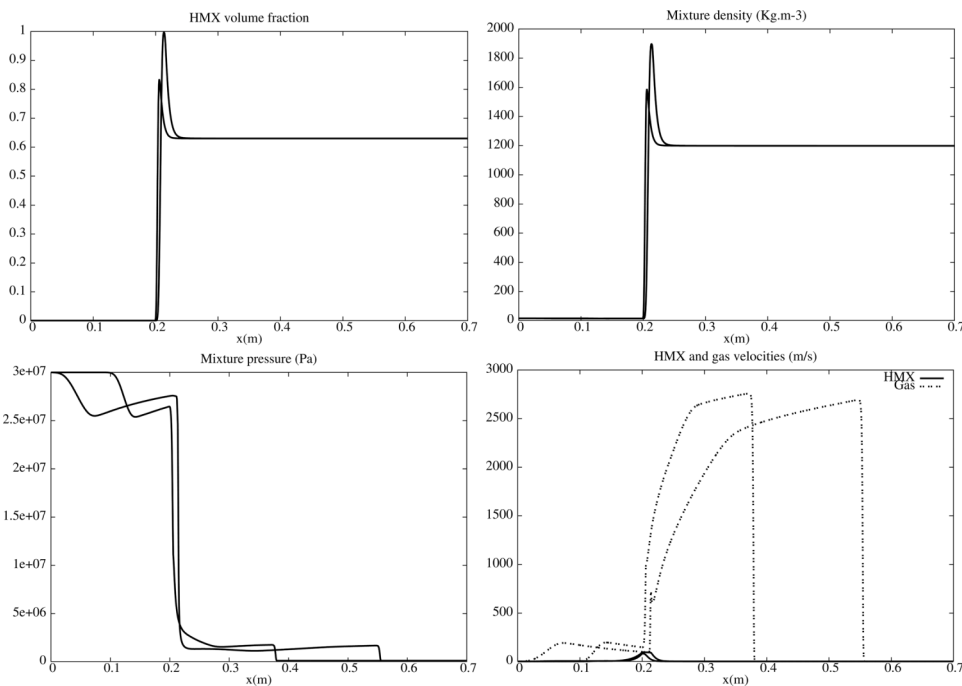


FIG. 11. Reference solution with a shock tube having a “pure” gas at left and a two-phase mixture at right in the absence of granular pressure. Volume fraction, mixture density, mixture pressure, and phase velocities profiles are shown at times 0.05 ms and 0.1 ms. The two pressures are relaxed. Huge velocity disequilibrium is present, except at the interface where the velocities merge, as the solid volume fraction reaches nearly 1.

We now consider granular effects with the granular EOS parameters given in Sec. II. The same initial conditions as previous are used. The results are shown at the same times in Figure 12.

As expected, gas in the high pressure chamber presses the granular media and granular pressure (~ 170 atm) appears, restraining the HMX volume fraction lower than 0.8. Moreover, the effects of this granular pressure can be seen in the pressure profiles as well as in the HMX velocity profile. Compared to the two fluids situation, an extra “granular” wave appears. We now address extra physics modelling to progress to the direction of reactive granular media simulations.

V. COMBUSTION MODELLING

To deal with combustion of granular energetic materials, several effects have to be considered through source terms that couple the two phases.

Let us consider System (2.10) expressed under compact form as

$$\frac{\partial \mathbf{U}}{\partial t} + \frac{\partial \mathbf{F}_{\text{eul}}}{\partial x} = \mathbf{F}_{\text{lag}} \frac{\partial \alpha_1}{\partial x} + \mathbf{S}(\mathbf{U}) \quad (5.1)$$

$$\text{with } \mathbf{U} = \begin{pmatrix} \alpha_1, & \alpha_1 \rho_1, & \alpha_1 \rho_1 u_1, & \alpha_1 \rho_1 E_1, & \alpha_2 \rho_2, & \alpha_2 \rho_2 u_2, & \alpha_2 \rho_2 E_2 \end{pmatrix}^T,$$

$$\mathbf{F}_{\text{eul}} = \begin{pmatrix} 0, & \alpha_1 \rho_1 u_1, & \alpha_1 \rho_1 u_1^2 + \alpha_1 p_1, & \alpha_1 (\rho_1 E_1 + p_1) u_1, & \alpha_2 \rho_2 u_2, & \alpha_2 \rho_2 u_2^2 + \alpha_2 p_2, & \alpha_2 (\rho_2 E_2 + p_2) u_2 \end{pmatrix}^T,$$

$$\mathbf{F}_{\text{lag}} = \begin{pmatrix} -u_1, & 0, & \pi_1, & \pi_1 u_1, & 0, & -\pi_1, & -\pi_1 u_1 \end{pmatrix}^T,$$

and

$$\mathbf{S}(\mathbf{U}) = \begin{pmatrix} \mu(\pi_1 - \pi_2), & 0, & 0, & -\mu\pi'_1(\pi_1 - \pi_2), & 0, & 0, & \mu\pi'_1(\pi_1 - \pi_2) \end{pmatrix}^T.$$

The velocity relaxation terms have been omitted as they will be examined in more details in the following. All source terms involve the specific interfacial exchange area A_I that needs additional information.

A. Interfacial area

System (5.1) is complemented by the number density of grain equation

$$\frac{\partial(\alpha \rho n)_1}{\partial t} + \frac{\partial(\alpha \rho n u)_1}{\partial x} = 0, \quad (5.2)$$

where n_1 represents the number density of grains per unit mass. Obviously,

$$(\alpha \rho n)_1 = N_1,$$

where N_1 represents the specific number of grains per unit volume. Formulation (5.2) is more convenient than

$$\frac{\partial N_1}{\partial t} + \frac{\partial(N u)_1}{\partial x} = 0,$$

when used with the DEM.

Grain fragmentation and coalescence are considered absent. From the knowledge of the volume fraction determined by the first equation of System (5.1) and number density n_1 determined by (5.2), there is no difficulty to determine the grain size that varies with both time and space, as a result of compressibility, dilatation, and obviously mass consumption. Considering spherical particles, their radius R_1 is determined by

$$\alpha_1 = \frac{4}{3}\pi R_1^3 N_1.$$

Then, the specific interfacial area A_I is deduced as

$$A_I = 4\pi R_1^2 N_1.$$

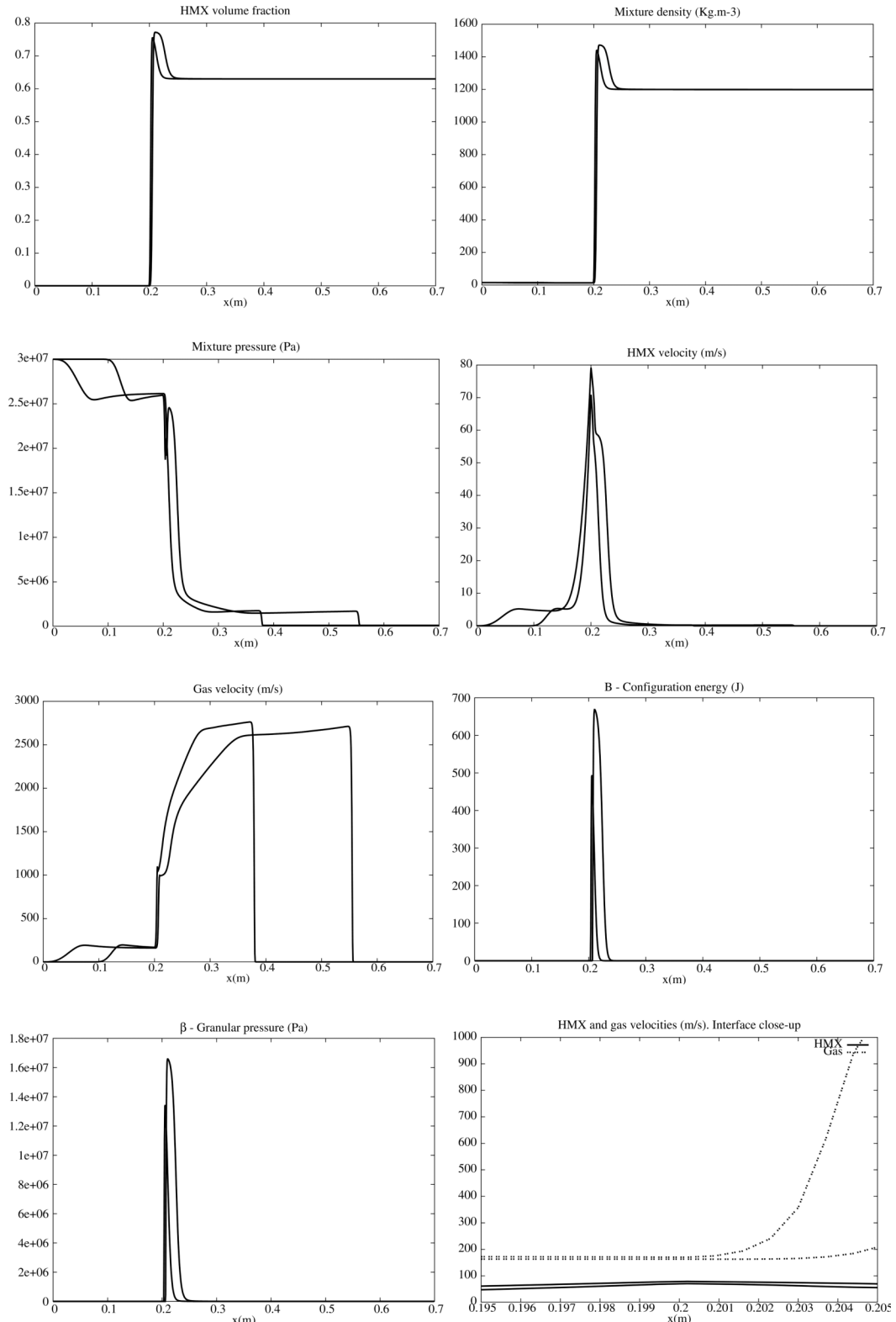


FIG. 12. Shock tube test with a “pure” gas at left and a granular media at right. Granular effects are now present. They clearly change the volume fraction evolution. Large velocity slip of the order of 100 m/s is present at the interface, as shown in the last graph. The granular interface is clearly permeable.

B. Drag exchanges

Drag exchanges are considered through the ODE system

$$\frac{\partial \mathbf{U}}{\partial t} = \mathbf{S}_D(\mathbf{U}),$$

with the source term vector

$$\mathbf{S}_D(\mathbf{U}) = \begin{pmatrix} 0, & 0, & F_D, & u'_I F_D, & 0, & -F_D, & -u'_I F_D \end{pmatrix}^T.$$

The specific drag force F_D is given by

$$F_D = A_I f_D,$$

where f_D is a drag correlation appropriate to dense packed granular beds. A well accepted correlation is given by Ergun²³ if the granular media is packed $\alpha_1 \geq \alpha_0$ and by Bernecker and Price²⁴ if the granular bed is fluidized,

$$f_D = \frac{1}{6(1-\alpha_1)} \rho_2 |u_2 - u_1| (u_2 - u_1) C_d.$$

C_d represents the drag coefficient, given by

$$C_d = \begin{cases} \frac{150\alpha_1}{Re} + 1.75 & \text{if } \alpha_1 \geq \alpha_0 \\ \frac{150\alpha_1}{Re} + 1.75 \left[\frac{(1-\alpha_0)\alpha_1}{(1-\alpha_1)\alpha_0} \right]^{0.45} & \text{if } \alpha_0 > \alpha_1 \geq (1-\alpha^*), \\ \frac{150\alpha_1}{Re} + 0.3 & \text{if } \alpha_1 < (1-\alpha^*) \end{cases}$$

with $\alpha^* = \left(1 + 0.02 \frac{\alpha_0}{1-\alpha_0}\right)^{-1}$.

In these formulas, the particle Reynolds number is expressed as $Re = \frac{2\alpha_2 \rho_2 R_1 |u_1 - u_2|}{\mu_{v2}}$.

C. Heat exchanges

Heat exchanges are considered through the ODE system,

$$\frac{\partial \mathbf{U}}{\partial t} = \mathbf{S}_H(\mathbf{U})$$

with the source term vector

$$\mathbf{S}_H(\mathbf{U}) = \begin{pmatrix} 0, & 0, & 0, & Q_1, & 0, & 0, & Q_2 \end{pmatrix}^T,$$

where

$$Q_1 = A_I h_1 (T_I - T_1),$$

$$Q_2 = A_I h_2 (T_I - T_2).$$

In the absence of mass transfer, the interface temperature is given by

$$T_I = \frac{h_1 T_1 + h_2 T_2}{h_1 + h_2}.$$

With this definition of T_I , $Q_1 + Q_2 = 0$.

The heat exchange coefficient on the gas side is given by an appropriate correlation

$$h_2 = \frac{\lambda_{T2} N u_2}{2 R_1},$$

where λ_{T2} represents the gas phase conductivity and $N u_2$ represents the gas phase Nusselt number. This last one is given by some correlation. If the granular media is dense ($\alpha_1 \geq \alpha_0$), the Denton

correlation (see Ref. 6) is used,

$$\text{Nu}_2 = 0.4 \left(\frac{R_e}{1 - \alpha_1} \right)^{0.7} P_r^{0.33}.$$

Otherwise, the Gelperin-Einstein correlation (see Ref. 5) is used,

$$\text{Nu}_2 = 2 + 0.4 \left(\frac{R_e}{1 - \alpha_1} \right)^{2/3} P_r^{0.33},$$

where P_r denotes the Prandtl number $P_r = \frac{\mu c_{p2}}{\lambda T_2}$ and c_{p2} denotes the gas specific heat at constant pressure.

Radiative heat transfers can be considered as well between the interface and the gas phase. The radiative heat flux reads

$$Q_R = A_I \varepsilon \sigma (T_I^4 - T_2^4), \quad (5.3)$$

where ε represents the emissivity and σ is the Stefan-Boltzmann constant ($\sigma = 5.67 \times 10^{-8} \text{ W m}^{-2} \text{ K}^{-4}$).

Expanding relation (5.3), a radiative heat exchange coefficient appears

$$Q_R = A_I \varepsilon \sigma (T_I^2 + T_2^2)(T_I + T_2)(T_I - T_2).$$

Therefore,

$$h_R = \varepsilon \sigma (T_I^2 + T_2^2)(T_I + T_2).$$

The heat exchange coefficient between the gas phase and the interface becomes

$$h_2 = \frac{\lambda_{T2} \text{Nu}_2}{2R_1} + h_R.$$

Determination of the heat exchange coefficient inside the particle (h_1) follows the approximate method given in Ref. 25 (p. 716). It results in the following particle internal heat exchange coefficient

$$h_1 = \frac{5\lambda_{T1}}{R_1}.$$

More sophisticated approximations are possible and will be detailed in forthcoming study dealing with hot spot ignition.

D. Mass exchanges

Mass exchanges are considered through the ODE system,

$$\frac{\partial U}{\partial t} = S_M(U),$$

with the source term vector

$$S(U) = \left(\frac{m}{\rho_I}, \quad m, \quad mu'_I, \quad mE_I, \quad -m, \quad -mu'_I, \quad -mE_I \right)^T.$$

When the interface temperature T_I exceeds a threshold temperature T^* (500 K for instance), particle combustion occurs. Immediately, the interface temperature takes the flame temperature $T_I = T_f$ (4000 K for instance). It is then no longer needed to account for the particle internal heat exchange as the thermal boundary layer is consumed by the flame front.

The mass transfer rate is expressed by the Vieille's law linking the particle regression rate to the pressure,

$$\frac{dR}{dt} = \dot{R}_1 = -AP^N.$$

The constants A and N are characteristic of a given propellant.

The mass transfer rate thus reads

$$\dot{m} = \rho_1 A_I \dot{R}_1.$$

As the regression rate is negative, the solid mass flow rate is negative too.

The interfacial velocity in these equations is still given by the acoustic approximation

$$u'_I = \frac{Z_1 u_1 + Z_2 u_2}{Z_1 + Z_2}.$$

As pressure relaxation is used systematically, appropriate modelling of ρ_I is obtained following the same method as in Ref. 26,

$$\rho_I = \frac{\frac{\rho_1 C_1^2}{\alpha_1} + \frac{\rho_2 C_2^2}{\alpha_2}}{\frac{c_1^2}{\alpha_1} + \frac{c_2^2}{\alpha_2} - \frac{dB_1}{d\alpha_1} - \frac{dB_2}{d\alpha_2}},$$

where $C_k^2 = c_k^2 + \alpha_k^2 \frac{d^2 B_k}{d\alpha_k^2}$.

It remains to provide an estimate for the interfacial energy E_I . This is the aim of Sec. V E.

E. Thermodynamic compatibility

First of all, as soon as mass transfer is considered, care has to be taken with internal energy definitions. Let us assume that both phases have constant specific heat at constant volume,

$$\begin{aligned} e_1 &= c_{v1} T_1 + \frac{p_{\infty 1}}{\rho_1} + q_1, \\ e_2 &= c_{v2} T_2 + q_2. \end{aligned}$$

The chemical reaction,

Reactive solid \rightarrow Gas products is exothermic. It means that

$$\Delta h_{\text{reaction}}^0 = h_2 - h_1 = (c_{p2} - c_{p1})T_0 + q_2 - q_1 - \frac{p_{\infty 1}}{\rho_1^0} = q_R < 0.$$

Usually, $(c_{p2} - c_{p1})T$ is negligible compared to the other terms. One of the reference energies has to be defined, q_1 or q_2 . We take the convention $q_2 = 0$.

Therefore,

$$q_1 = -q_R - \frac{p_{\infty 1}}{\rho_1^0}.$$

Usually, the chemical heat release is determined experimentally. For example, $q_R = -6 \times 10^6 \text{ J/kg}$. As for condensed materials p_∞ is big, non-negligible correction has to be done to the reference energy,

$$q_1 = 6 \times 10^6 - \frac{6 \times 10^8}{1000} = 5.4 \times 10^6 \text{ J/kg}.$$

As a prototype EOS, the stiffened gas EOS for the solid phase is qualitatively accurate enough. Regarding the gas phase EOS, covolume effects are mandatory. The simplest EOS in this frame is the Noble-Abel one,

$$p_2 = \frac{(\gamma_2 - 1)\rho_2(e_2 - q_2)}{1 - \eta\rho_2}.$$

The caloric EOS,

$$e_2 = c_{v2} T_2 + q_2,$$

is in agreement with the above thermal EOS with respect to Maxwell relations. The covolume is denoted by η .

We now examine source terms agreement with the second law of thermodynamics. The flow model reads for phase 1:

$$\begin{aligned} \frac{\partial \alpha_1}{\partial t} + u_I \frac{\partial \alpha_1}{\partial x} &= \mu(\pi_1 - \pi_2) + \frac{m}{\rho_I}, \\ \frac{\partial(\alpha\rho)_1}{\partial t} + \frac{\partial(\alpha\rho u)_1}{\partial x} &= m, \\ \frac{\partial(\alpha\rho u)_1}{\partial t} + \frac{\partial(\alpha\rho u^2 + \alpha p)_1}{\partial x} &= \pi_I \frac{\partial \alpha_1}{\partial x} + F_D + mu'_I, \\ \frac{\partial(\alpha\rho E)_1}{\partial t} + \frac{\partial(\alpha(\rho E + p)u)_1}{\partial x} &= \pi_I u_I \frac{\partial \alpha_1}{\partial x} + F_D u'_I - \mu \pi'_I (\pi_1 - \pi_2) + Q_1 + mE_I. \end{aligned} \quad (5.4)$$

Mass transfer being considered, drag force is assumed to be function of the friction coefficient (λ) and mass transfer (m),

$$F_D = (\lambda + \omega m)(u_2 - u_1),$$

the parameter ω being to determine.

System (5.4) is expressed in primitive variables formulation:

$$\begin{aligned} \frac{d_I \alpha_1}{dt} &= -(u_I - u_1) \frac{\partial \alpha_1}{\partial x} + \mu(\pi_1 - \pi_2) + \frac{m}{\rho_I}, \\ \frac{\partial u_1}{\partial x} &= \frac{m}{\alpha_1} \left(\frac{1}{\rho_1} - \frac{1}{\rho_I} \right) + \frac{(u_I - u_1)}{\alpha_1} \frac{\partial \alpha_1}{\partial x} - \frac{\mu(\pi_1 - \pi_2)}{\alpha_1} - \frac{1}{\rho_1} \frac{d_I \rho_1}{dt}, \\ (\alpha\rho)_1 \frac{d_I u_1}{dt} &= -\alpha_1 \frac{\partial p_1}{\partial x} + (\pi_I - p_1) \frac{\partial \alpha_1}{\partial x} + (\lambda + \omega m)(u_2 - u_1) + m(u'_I - u_1), \\ (\alpha\rho)_1 T_1 \frac{d_I s_1}{dt} &= (\pi_I - \pi_1)(u_I - u_1) \frac{\partial \alpha_1}{\partial x} + \lambda(u_2 - u_1)(u'_I - u_1) - \mu(\pi_1 - \pi_2)(\pi'_I - \pi_1) + Q_1 \\ &\quad + m \left(E_I + \frac{\pi_1}{\rho_1} - E_1 - \frac{p_1}{\rho_1} + (u'_I - u_1)(\omega(u_2 - u_1) - u_1) \right). \end{aligned}$$

It suggests

$$E_I = E_1 + \frac{p_1}{\rho_1} - \frac{\pi_1}{\rho_1} - (u'_I - u_1)(\omega(u_2 - u_1) - u_1). \quad (5.5)$$

The phase 1 entropy equation becomes

$$(\alpha\rho)_1 T_1 \frac{d_I s_1}{dt} = (\pi_I - \pi_1)(u_I - u_1) \frac{\partial \alpha_1}{\partial x} + \lambda(u_2 - u_1)(u'_I - u_1) - \mu(\pi_1 - \pi_2)(\pi'_I - \pi_1) + Q_1.$$

Following the calculations done with System (2.10), all production terms are positive or null except the heat transfer term Q_1 .

The second phase entropy equation reads

$$\begin{aligned} (\alpha\rho)_2 T_2 \frac{d_2 s_2}{dt} &= (\pi_I - \pi_2)(u_I - u_2) \frac{\partial \alpha_2}{\partial x} + \lambda(u_1 - u_2)(u'_I - u_2) - \mu(\pi_2 - \pi_1)(\pi'_I - \pi_2) + Q_2 \\ &\quad - m \left(E_I + \frac{\pi_2}{\rho_1} - E_2 - \frac{p_2}{\rho_2} + (u'_I - u_2)(\omega(u_1 - u_2) - u_2) \right). \end{aligned}$$

All production terms are positive or null, except Q_2 and the term related to mass transfer. Let us examine this last term. Using the estimate for E_I it becomes

$$-m \left(E_1 + \frac{p_1}{\rho_1} - \frac{\pi_1}{\rho_1} - (u'_I - u_1)(\omega(u_2 - u_1) - u_1) + \frac{\pi_2}{\rho_1} - E_2 - \frac{p_2}{\rho_2} + (u'_I - u_2)(\omega(u_1 - u_2) - u_2) \right).$$

It suggests

$$\omega = -\frac{1}{2}$$

in agreement with the Kapila *et al.*⁸ formulation of drag.

The term related to mass transfer in the entropy equation for phase 2 thus reduces to

$$-m \left(h_1 - h_2 + B_1 + \frac{\pi_2 - \pi_1}{\rho_I} \right).$$

The “granular” energy B_1 is negligible compared to the enthalpy h_1 . Considering the stiff stress relaxation limit the production term becomes

$$-m(h_1 - h_2).$$

The heat of reaction being exothermic, $h_1 - h_2 > 0$, and as the mass flow rate being negative (the solid transforms to gas $m < 0$), the entropy production term related to mass transfer is positive.

Consequently, with the definition (5.5), the interfacial variables defined with System (2.10) and the definitions for Q_1 , Q_2 , and T_1 , the mixture entropy evolution reads

$$\begin{aligned} \frac{\partial(\alpha\rho)_1 s_1 + (\alpha\rho)_2 s_2}{\partial t} + \frac{\partial(\alpha\rho)_1 u_1 s_1 + (\alpha\rho)_2 u_2 s_2}{\partial x} &= A_I \frac{h_1 h_2}{h_1 + h_2} \frac{(T_2 - T_1)^2}{T_1 T_2} \\ \frac{1}{T_1} \left\{ \frac{Z_1}{(Z_1 + Z_2)^2} \left((\pi_2 - \pi_1) + \text{sgn} \left(\frac{\partial a_1}{\partial x} \right) Z_2(u_2 - u_1) \right)^2 \left| \frac{\partial a_1}{\partial x} \right| + \lambda \frac{Z_2}{Z_1 + Z_2} (u_2 - u_1)^2 + \mu \frac{Z_1}{Z_1 + Z_2} (\pi_2 - \pi_1)^2 \right\} \\ + \frac{1}{T_2} \left\{ \frac{Z_2}{(Z_1 + Z_2)^2} \left((\pi_2 - \pi_1) + \text{sgn} \left(\frac{\partial a_1}{\partial x} \right) Z_2(u_2 - u_1) \right)^2 \left| \frac{\partial a_2}{\partial x} \right| + \lambda \frac{Z_1}{Z_1 + Z_2} (u_2 - u_1)^2 + \mu \frac{Z_2}{Z_1 + Z_2} (\pi_2 - \pi_1)^2 \right\}, \\ -m \left(g_1 - g_2 + (T_1 - T_2)s_1 + B_1 + \frac{1}{\rho_I}(\pi_2 - \pi_1) \right) \end{aligned}$$

where $g_k = h_k - T_k s_k$ denotes the Gibbs free energy of phase k .

Except regarding the entropy production due to mass transfer that is a solid-gas irreversible reaction, all terms are symmetric. The final flow model with granular combustion is thus summarized hereafter.

F. Final model of reactive granular media

The system modelling granular combustion, gas permeation (in particular through two-phase interfaces) and compaction effects is expressed hereafter

$$\begin{aligned} \frac{\partial a_1}{\partial t} + u_I \frac{\partial a_1}{\partial x} &= \mu(\pi_1 - \pi_2) + \frac{m}{\rho_I}, \\ \frac{\partial(\alpha\rho)_1}{\partial t} + \frac{\partial(\alpha\rho u)_1}{\partial x} &= m, \\ \frac{\partial(\alpha\rho n)_1}{\partial t} + \frac{\partial(\alpha\rho n u)_1}{\partial x} &= 0, \\ \frac{\partial(\alpha\rho u)_1}{\partial t} + \frac{\partial(\alpha\rho u^2 + \alpha p)_1}{\partial x} &= \pi_I \frac{\partial a_1}{\partial x} + F_D + mu'_I, \\ \frac{\partial(\alpha\rho E)_1}{\partial t} + \frac{\partial(\alpha(\rho E + p)u)_1}{\partial x} &= \pi_I u_I \frac{\partial a_1}{\partial x} + F_D u'_I - \mu \pi'_I (\pi_1 - \pi_2) + Q_1 + mE_I, \\ \frac{\partial(\alpha\rho)_2}{\partial t} + \frac{\partial(\alpha\rho u)_2}{\partial x} &= -m, \\ \frac{\partial(\alpha\rho u)_2}{\partial t} + \frac{\partial(\alpha\rho u^2 + \alpha p)_2}{\partial x} &= \pi_I \frac{\partial a_2}{\partial x} - F_D - mu'_I, \\ \frac{\partial(\alpha\rho E)_2}{\partial t} + \frac{\partial(\alpha(\rho E + p)u)_2}{\partial x} &= \pi_I u_I \frac{\partial a_2}{\partial x} - F_D u'_I + \mu \pi'_I (\pi_1 - \pi_2) + Q_2 - mE_I. \end{aligned} \quad (5.6)$$

It is closed by the following set of relations.

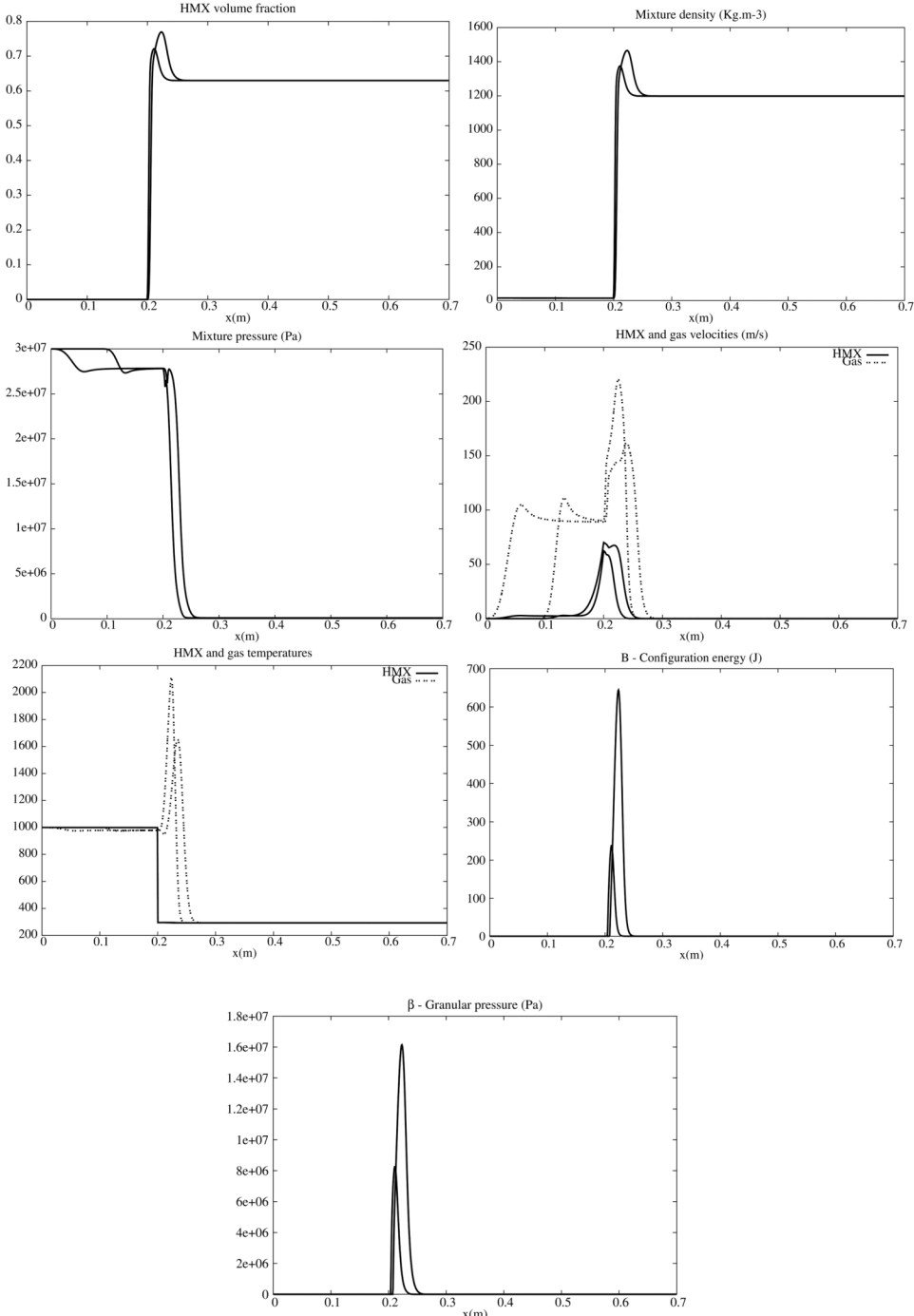


FIG. 13. Two-phase flow variable evolutions for the shock tube test problem in the presence of granular pressure, drag force, and heat exchanges. The drag force clearly reduces velocity drift, modifying the granular pressure and mixture pressure profiles. The heat exchange lowers the temperature difference modifying in turn the granular and mixture pressures.

Mechanical interfacial variables

$$u_I = u'_I + \text{sgn} \left(\frac{\partial a_1}{\partial x} \right) \frac{\pi_2 - \pi_1}{Z_1 + Z_2}, \quad u'_I = \frac{Z_1 u_1 + Z_2 u_2}{Z_1 + Z_2},$$

$$\pi_I = \pi'_I + \text{sgn} \left(\frac{\partial a_1}{\partial x} \right) \frac{Z_1 Z_2}{Z_1 + Z_2} (u_2 - u_1), \quad \pi'_I = \frac{Z_2 \pi_1 + Z_1 \pi_2}{Z_1 + Z_2}.$$

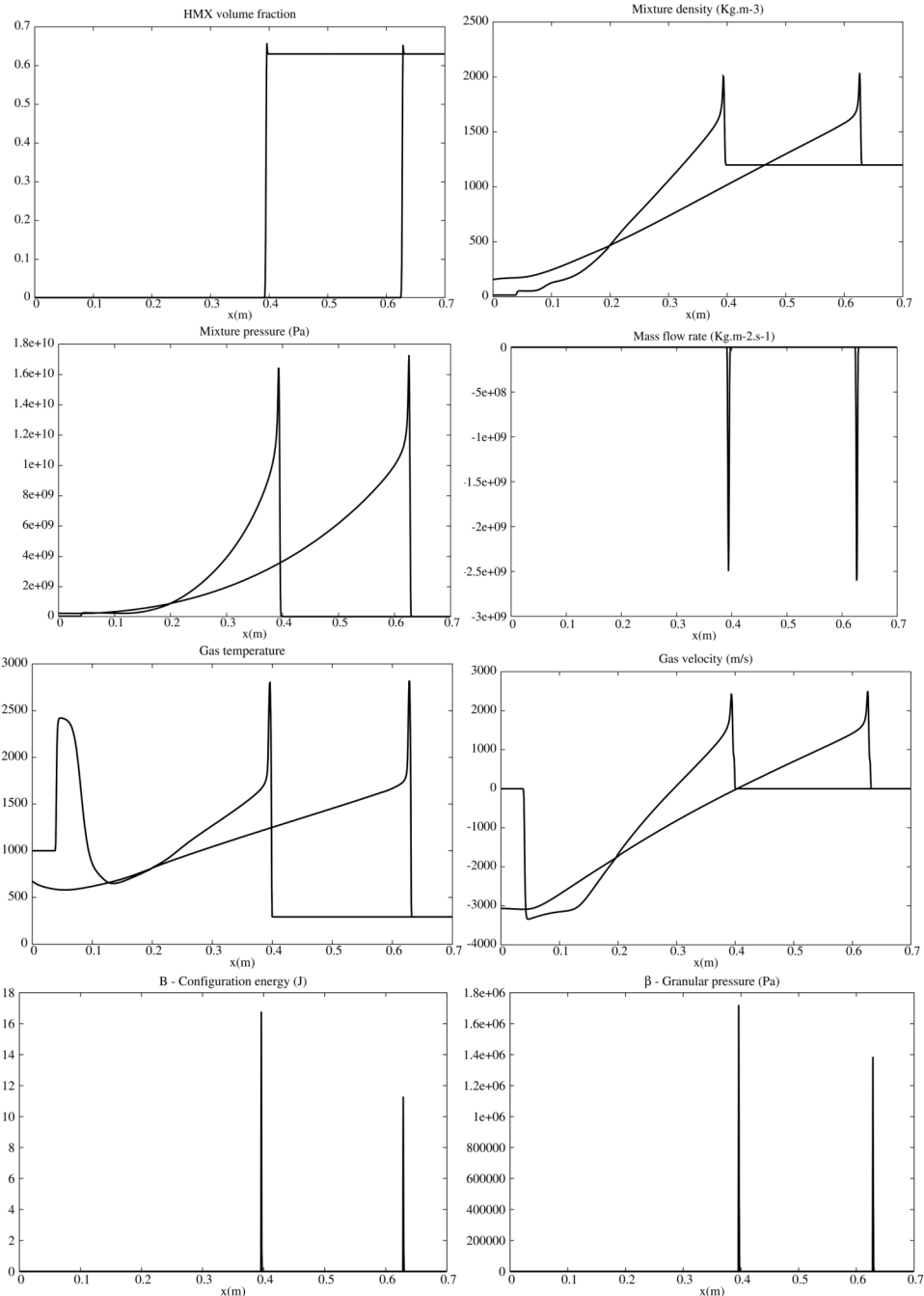


FIG. 14. Two-phase flow variables for the same test as previously in the presence of mass transfer. A detonation wave appears.

Interfacial area

$$(\alpha \rho n)_I = N_1, \quad \alpha_I = \frac{4}{3} \pi R_1^3 N_1, \text{ and } A_I = 4\pi R_1^2 N_1.$$

Heat transfer

$$Q_1 = A_I h_{T1} (T_I - T_1), \quad Q_2 = A_I h_{T2} (T_I - T_2), \quad T_I = \frac{h_{T1} T_1 + h_{T2} T_2}{h_{T1} + h_{T2}},$$

$$h_{T1} = \frac{5\lambda_{T1}}{R_1}, \quad h_{T2} = \frac{\lambda_{T2} N u_2}{2R_1} + h_R, \quad h_R = \varepsilon \sigma (T_I^2 + T_2^2) (T_I + T_2),$$

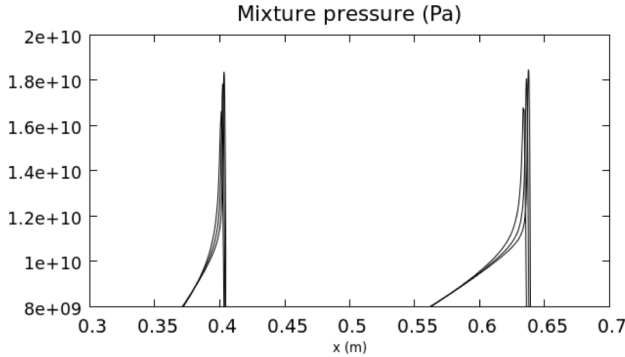


FIG. 15. Computed pressure profiles near the Neumann spike with 1000, 2000, and 4000 cells showing convergence of the results. Computations with 1000 cells appear as good compromise.

$$\text{Nu}_2 = \begin{cases} 0.4 \left(\frac{R_e}{1 - \alpha_1} \right)^{0.7} P_r^{0.33} & \text{if } \alpha_1 \geq \alpha_0 \\ 2 + 0.4 \left(\frac{R_e}{1 - \alpha_1} \right)^{2/3} P_r^{0.33} & \text{otherwise} \end{cases},$$

and $P_r = \frac{\mu_{v2} c p_2^2}{\lambda_{T2}}$.

Momentum transfer

$$\begin{aligned} F_D &= A_I f_D - \frac{1}{2} m, \\ f_D &= \frac{1}{6(1 - \alpha_1)} \rho_2 |u_2 - u_1| (u_2 - u_1) C_d, \\ C_d &= \begin{cases} \frac{150\alpha_1}{Re} + 1.75 & \text{if } \alpha_1 \geq \alpha_0 \\ \frac{150\alpha_1}{Re} + 1.75 \left[\frac{(1 - \alpha_0)\alpha_1}{(1 - \alpha_1)\alpha_0} \right]^{0.45} & \text{if } \alpha_0 > \alpha_1 \geq (1 - \alpha^*), \\ \frac{150\alpha_1}{Re} + 0.3 & \text{if } \alpha_1 < (1 - \alpha^*) \end{cases}, \\ \alpha^* &= \left(1 + 0.02 \frac{\alpha_0}{1 - \alpha_0} \right)^{-1}, \quad Re = \frac{2\alpha_2 \rho_2 R_1 |u_1 - u_2|}{\mu_{v2}}. \end{aligned}$$

Mass transfer

$$\begin{aligned} m &= \rho_1 A_I \dot{R}_1, \quad \dot{R}_1 = -a P^n, \\ \rho_I &= \frac{\frac{\rho_1 C_1^2}{\alpha_1} + \frac{\rho_2 C_2^2}{\alpha_2}}{\frac{c_1^2}{\alpha_1} + \frac{c_2^2}{\alpha_2} - \frac{dB_1}{d\alpha_1} - \frac{dB_2}{d\alpha_2}}, \end{aligned}$$

and $E_I = E_1 + \frac{p_1}{\rho_1} - \frac{\pi_1}{\rho_I} + \frac{u_2 + u_1}{2}(u'_I - u_I)$.

Equations of state

$$\begin{aligned} p_1 &= (\gamma_1 - 1)\rho_1(e_1 - q_1) - \gamma_1 p_{\infty 1}, \quad p_2 = \frac{(\gamma_2 - 1)\rho_2(e_2 - q_2)}{1 - \eta\rho_2}, \\ e_1 &= c_{v1} T_1 + \frac{p_{\infty 1}}{\rho_1} + q_1, \quad e_2 = c_{v2} T_2 + q_2, \\ \Delta h_{\text{reaction}}^0 &= h_2 - h_1 = (c_{p2} - c_{p1})T_0 + q_2 - q_1 - \frac{p_{\infty 1}}{\rho_1^0} \cong q_R < 0, \\ q_1 &= -q_R - \frac{p_{\infty 1}}{\rho_1^0}. \end{aligned}$$

System (5.6) is hyperbolic, symmetric, and thermodynamically consistent.

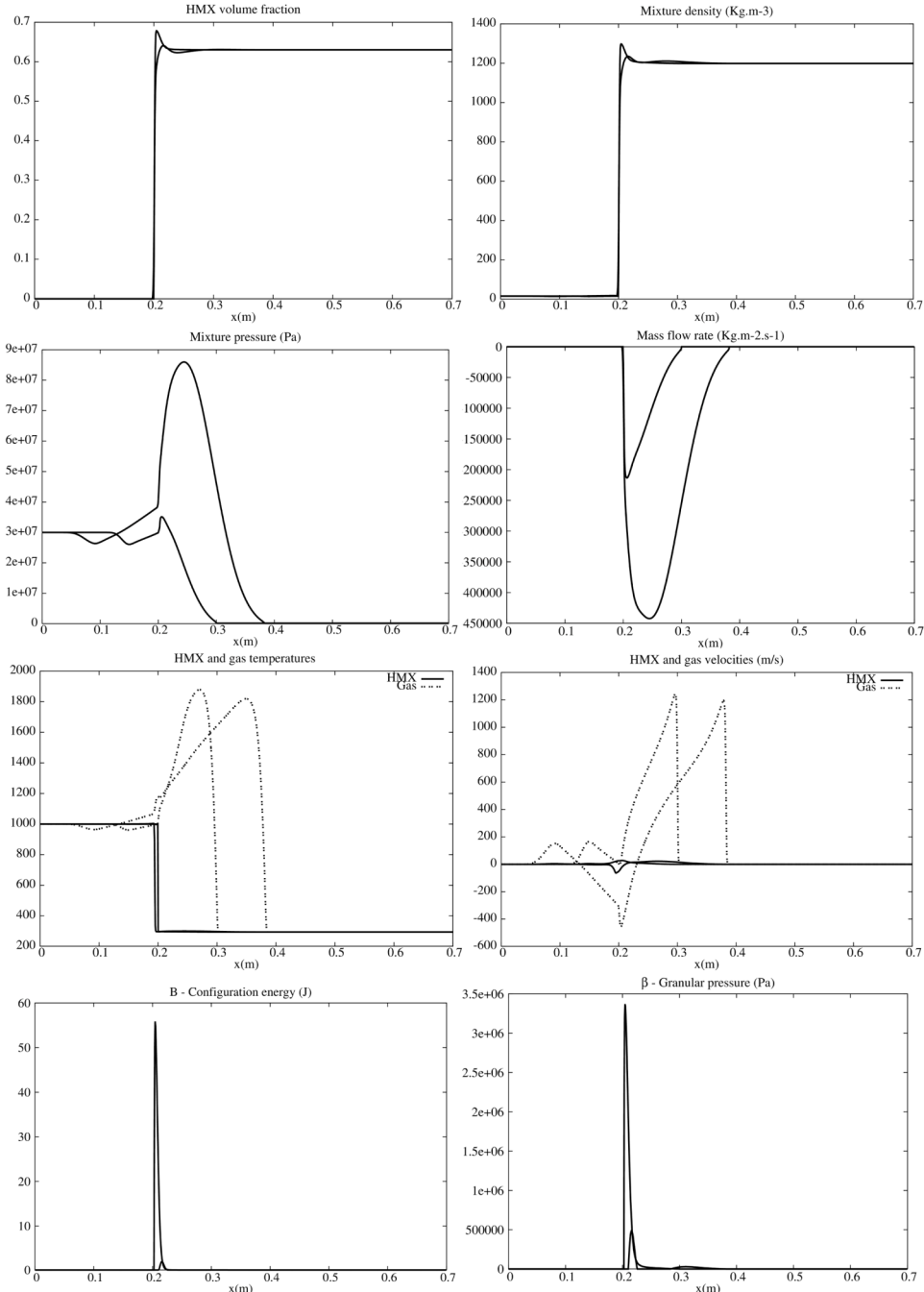


FIG. 16. Two-phase flow variables for the same test as previous except regarding particles' size now increased by a factor 50, decreasing the specific interfacial area. The detonation wave disappears but a fast deflagration wave appears, resulting in hot gas and particles flow in direction opposite to the front.

VI. ILLUSTRATIONS

We now consider the same shock tube test problem as presented in Sec. IV. From these reference results, extra physics is added gradually in the direction of combustion modelling.

All runs consider particles of initial radius equal to 0.5 mm everywhere and the results are shown at time 0.05 ms and 0.1 ms.

First, drag force and heat transfers are considered, with following transport properties: $\mu_{v2} = 50 \times 10^{-6}$ Pa/s (air viscosity), $\lambda_{HMX} = 2.8 \text{ W m}^{-1} \text{ K}^{-1}$, and $\lambda_{AIR} = 0.002818 \text{ W m}^{-1} \text{ K}^{-1}$ (thermal conductivities). The HMX radiative emissivity is estimated as $\epsilon = 0.8$. Figure 13 shows corresponding results.

Then, mass transfer is added. Corresponding results are shown in Figure 14 at times 0.04 ms and 0.08 ms (different of the previous times) as the process dynamics is substantially changed.

Mass transfer with combination of previous ingredients yields to a detonation wave (moving at 5809 m/s) showing a fast ignition and deflagration to detonation transition. As shown in the Figure 14, the HMX is almost completely burnt while fast and hot gases are ejected towards the left boundary. The last graphs of Figure 14 show the configuration energy and granular pressure spikes that coincide with the von Neumann spike. Mesh convergence of the results is shown in Figure 15 with close up views of pressure profiles near the Neumann spike, reaction zone, and expansion wave.

Last, in order to show that the modelling and the numerical algorithms can also handle slower combustion waves, a test case of “fast deflagration” or “convective burning” is examined. The same parameters as previous are used, except regarding particles’ size, that is magnified by a factor 50 (particle radius is now equal to 2.5 cm). Results are shown at the same times as in the previous case, 0.04 ms and 0.08 ms in Figure 16.

Increasing the particle size decreases the interfacial area resulting in detonation disappearance, at least for the present domain dimensions. However, hot gases are present, moving at high speed (about 500 m/s) in direction opposite to the deflagration front that propagates to the right at a speed close to acoustic waves (about 2 km/s). Such convective burning mode may result in damages with comparable dramatic effects as the detonation mode.

VII. CONCLUSION

A symmetric Baer and Nunziato type model has been built to model two-phase mixtures in the presence of gas permeation, “granular” pressure, heat and mass transfers, and material interfaces, as well as two-phase interfaces. Its capabilities have been demonstrated on several test problems showing enhanced capabilities compared to existing models.

The next step will be to assemble pore collapse and inner pore combustion (Kang *et al.*²⁷ and Massoni *et al.*²⁵) in this frame to deal with a wider range of ignition and combustion modes of solid energetic materials.

ACKNOWLEDGMENTS

Part of this work has been carried out in the framework of the Labex MEC (ANR-10-LABX-0092) and of the A*MIDEX project (ANR-11-IDEX-0001-02), funded by the “Investissements d’Avenir” French Government program managed by the National Research Agency (ANR). The authors are also grateful to the anonymous referee for the quality of their reports that helped to improve significant quality of the manuscript.

APPENDIX A: STIFF MECHANICAL RELAXATION SOLVERS

1. Stiff velocity relaxation solver

The following system is considered in the limit of stiff velocity relaxation ($\lambda \rightarrow +\infty$):

$$\begin{aligned} \frac{\partial \alpha_1}{\partial t} &= 0, \\ \frac{\partial(\alpha\rho)_1}{\partial t} &= 0; \quad \frac{\partial(\alpha\rho)_2}{\partial t} = 0, \\ \frac{\partial(\alpha\rho u)_1}{\partial t} &= \lambda(u_2 - u_1); \quad \frac{\partial(\alpha\rho u)_2}{\partial t} = -\lambda(u_2 - u_1), \end{aligned}$$

$$\frac{\partial(\alpha\rho E)_1}{\partial t} = \lambda u'_I(u_2 - u_1); \quad \frac{\partial(\alpha\rho E)_2}{\partial t} = -\lambda u'_I(u_2 - u_1).$$

It implies

$$\begin{aligned} (\alpha\rho)_k &= \text{cst} \\ \rho &= (\alpha\rho)_1 + (\alpha\rho)_2 = \text{cst}, \\ Y_k &= \frac{(\alpha\rho)_k}{\rho} = \text{cst} \end{aligned}$$

where Y_k represents the mass fraction of phase k .

Considering the mixture momentum conservation, we obtain

$$\frac{\partial(\alpha\rho u)_1}{\partial t} + \frac{\partial(\alpha\rho u)_2}{\partial t} = \lambda(u_2 - u_1) - \lambda(u_2 - u_1) = 0.$$

Thus,

$$(\alpha\rho u)_1 + (\alpha\rho u)_2 = \text{cst}$$

or, using the mixture mass conservation,

$$(Yu)_1 + (Yu)_2 = \text{cst}.$$

This last relation means that the centre of mass velocity is constant during the relaxation process. Therefore, denoting by “0” the initial state, the velocity at relaxed state reads $u = (Yu)_1^0 + (Yu)_2^0$.

Update has to be done to the internal energies, as friction induces dissipation. Considering the phase energy, momentum, and mass equations, it appears

$$\frac{\partial E_k}{\partial t} = u_I \frac{\partial u_k}{\partial t}.$$

Assuming the interface velocity as constant and equal to the centre of mass velocity, $u_I = u = \text{cst}$, time integration of the previous relations results in

$$E_k = E_k^0 + u(u - u_k^0).$$

In terms of internal energies they read

$$e_k = e_k^0 + \frac{1}{2}(u - u_k^0)^2.$$

2. Stiff mechanical stress relaxation solver

The method given in Saurel *et al.*¹⁴ is adapted. It consists in solving the differential system:

$$\begin{aligned} \frac{\partial a_1}{\partial t} &= \mu(\pi_1 - \pi_2), \\ \frac{\partial(\alpha\rho)_1}{\partial t} &= 0; \quad \frac{\partial(\alpha\rho)_2}{\partial t} = 0, \\ \frac{\partial(\alpha\rho u)_1}{\partial t} &= 0; \quad \frac{\partial(\alpha\rho u)_2}{\partial t} = 0, \\ \frac{\partial(\alpha\rho)_1(e + B)_1}{\partial t} &= -\pi_I \mu(\pi_1 - \pi_2); \quad \frac{\partial(\alpha\rho)_2(e + B)_2}{\partial t} = \pi_I \mu(\pi_1 - \pi_2) \end{aligned}$$

in the limit $\mu \rightarrow +\infty$ and with $\pi_I = \frac{Z_2\pi_1 + Z_1\pi_2}{Z_1 + Z_2}$.

The kinetic energies have been removed in the total energy equation of each phase as velocities are constant during the relaxation step.

As only the equilibrium solution is required, the aim is to replace this ordinary differential system by an algebraic one. After some manipulations, the energy equations become

$$\frac{\partial(e_k + B_k)}{\partial t} + \pi_I \frac{\partial v_k}{\partial t} = 0,$$

where $v_k = 1/\rho_k$.

Upon integration, it becomes

$$(e_k + B_k) - (e_k^0 + B_k^0) + \hat{\pi}_{Ik}(v_k - v_k^0) = 0$$

$$\text{with } \hat{\pi}_{Ik} = \frac{1}{v_k - v_k^0} \int_0^{\Delta t} \pi_I \frac{\partial v_k}{\partial t} dt.$$

Following Saurel *et al.*,¹⁷ the interfacial pressure average can be estimated with sufficient accuracy by

$$\hat{\pi}_{Ik} = \pi$$

that represents the “pressure” in the equilibrium state.

The system to solve is thus composed of equations

$$e_k(p, v_k) + B_k(\alpha_k, \rho_k) - e_k^0(p_k^0, v_k^0) - B_k(\alpha_k^0, \rho_k^0) + \pi(v_k - v_k^0) = 0, \quad k = 1, 2. \quad (\text{A1})$$

The apparent densities $(\alpha\rho)_k$ remain constants during the relaxation process. Also, the volume fractions can be expressed as $\alpha_k = (\alpha\rho)_k^0 v_k$. System (A1) consequently becomes

$$e_k(p, v_k) + B_k(v_k) - e_k^0(p_k^0, v_k^0) - B_k(v_k^0) + \pi(v_k - v_k^0) = 0.$$

This system involves 3 unknowns v_k ($k = 1, 2$) and the equilibrium stress π . Its closure is achieved by the saturation condition

$$\sum_k \alpha_k = 1.$$

It is more convenient to express this condition as

$$\sum_k (\alpha\rho)_k v_k = 1. \quad (\text{A2})$$

To be more explicit, let us take the example of materials governed by the stiffened gas EOS. The internal energy in (A1) is replaced by a function of pressure and specific volume,

$$e_k = \frac{p_k + \gamma_k p_{\infty k}}{\rho_k(\gamma_k - 1)}.$$

The pressures in each phase are expressed with the help of the equilibrium condition as functions of π : $p_k = \pi + \beta_k(\alpha_k, \rho_k)$.

System (A1) becomes

$$\frac{(\pi + \beta_k + \gamma_k p_{\infty k}) v_k}{(\gamma_k - 1)} + B_k - \frac{(p_k^0 + \gamma_k p_{\infty k}) v_k^0}{(\gamma_k - 1)} - B_k^0 + \pi(v_k - v_k^0) = 0.$$

Note that in state 0, corresponding to the end of the hyperbolic step, the equilibrium pressure π has not been used as the state if out of mechanical equilibrium.

After some manipulations, we have

$$v_k = \frac{(p_k^0 + \gamma_k p_{\infty k} + (\gamma_k - 1)\pi) v_k^0 + (\gamma_k - 1)(B_k^0 - B_k)}{\beta_k + \gamma_k(\pi + p_{\infty k})}.$$

As this equation involves functions $\beta_k(\alpha_k, \rho_k)$ and $B_k(\alpha_k, \rho_k)$ that can be written as $\beta_k(v_k)$ and $B_k(v_k)$, the preceding equation becomes a function to solve for the determination of specific volume v_k . For a given estimate of the equilibrium “pressure” π , specific volumes v_k are solution of this equation. The pressure estimate is correct if the constraint,

$$\sum_k (\alpha\rho)_k v_k = 1,$$

is fulfilled. The Newton method is appropriate for such tasks.

APPENDIX B: NOBLE-ABEL EOS

The Noble-Abel EOS reads

$$p(\rho, e) = \frac{(\gamma - 1)\rho(e - q)}{1 - \eta\rho} \text{ and } e(T) = c_v T + q.$$

Combining these two equations of state, the pressure is expressed as a function of temperature and density,

$$p(\rho, T) = \frac{(\gamma - 1)\rho c_v T}{1 - \eta\rho}.$$

The square sound speed reads

$$c^2 = p(\gamma - \eta\rho) / (\rho(1 - \eta\rho)).$$

- ¹ B. W. Asay, S. F. Son, and J. B. Bdzip, "The role of gas permeation in convective burning," *Int. J. Multiphase Flow* **22**(5), 923–952 (1996).
- ² K. Andreev, "The problem of the mechanism of the transition from burning to detonation in explosives," *J. Phys. Chem.* **17**, 533–537 (1944).
- ³ J. B. Bdzip, R. Menikoff, S. F. Son, A. K. Kapila, and D. S. Stewart, "Two-phase modeling of deflagration-to-detonation transition in granular materials: A critical examination of modeling issues," *Phys. Fluids* **11**, 378 (1999).
- ⁴ M. R. Baer and J. W. Nunziato, "A two-phase mixture theory for the deflagration-to-detonation transition (DDT) in reactive granular materials," *Int. J. Multiphase Flow* **12**(6), 861–889 (1986).
- ⁵ H. Krier, S. Rajan, and W. F. Van Tassel, "Flame spreading and combustion in packed beds of propellant grains," *AIAA J.* **14**(3), 301–309 (1976).
- ⁶ P. S. Gough and F. J. Zwartz, "Modeling heterogeneous two-phase reacting flow," *AIAA J.* **17**(1), 17–25 (1979).
- ⁷ R. Saurel and R. Abgrall, "A multiphase Godunov method for compressible multifluid and multiphase flows," *J. Comput. Phys.* **150**, 425–467 (1999).
- ⁸ A. K. Kapila, R. Menikoff, J. B. Bdzip, S. F. Son, and D. S. Stewart, "Two-phase modeling of deflagration to detonation transition in granular materials: Reduced equations," *Phys. Fluids* **13**(10), 3002–3024 (2001).
- ⁹ R. Abgrall and R. Saurel, "Discrete equations for physical and numerical compressible multiphase mixtures," *J. Comput. Phys.* **186**(2), 361–396 (2003).
- ¹⁰ R. Saurel, S. Gavrilyuk, and F. Renaud, "A multiphase model with internal degrees of freedom: Application to shock-bubble interaction," *J. Fluid Mech.* **495**(1), 283–321 (2003).
- ¹¹ A. Chinnayya, E. Daniel, and R. Saurel, "Modelling detonation waves in heterogeneous energetic materials," *J. Comput. Phys.* **196**(2), 490–538 (2004).
- ¹² O. Le Métayer, J. Massoni, and R. Saurel, "Modelling evaporation fronts with reactive Riemann solvers," *J. Comput. Phys.* **205**(2), 567–610 (2005).
- ¹³ R. A. Berry, R. Saurel, and O. Lemetayer, "The discrete equation method (DEM) for fully compressible, two-phase flows in ducts of spatially varying cross-section," *Nucl. Eng. Des.* **240**(11), 3797–3818 (2010).
- ¹⁴ R. Saurel, N. Favrie, F. Petitpas, M. H. Lallemand, and S. Gavrilyuk, "Modelling dynamic and irreversible powder compaction," *J. Fluid Mech.* **664**, 348–396 (2010).
- ¹⁵ K. K. Kuo, V. Yang, and B. B. Moore, "Intragranular stress particle-wall friction and speed of sound in granular propellant beds," *J. Ballist.* **4**(1), 697–730 (1980).
- ¹⁶ A. K. Kapila, S. F. Son, J. B. Bdzip, R. Menikoff, and D. S. Stewart, "Two-phase modeling of DDT: Structure of the velocity-relaxation zone," *Phys. Fluids* **9**(12), 3885–3897 (1997).
- ¹⁷ R. Saurel, O. Le Metayer, J. Massoni, and S. Gavrilyuk, "Shock jump relations for multiphase mixtures with stiff mechanical relaxation," *Shock Waves* **16**(3), 209–232 (2007).
- ¹⁸ D. W. Schwendeman, C. W. Wahle, and A. K. Kapila, "The Riemann problem and a high-resolution Godunov method for a model of compressible two-phase flow," *J. Comput. Phys.* **212**(2), 490–526 (2006).
- ¹⁹ E. F. Toro, M. Spruce, and W. Speares, "Restoration of the contact surface in the HLL -Riemann solver," *Shock waves* **4**(1), 25–34 (1994).
- ²⁰ S. K. Godunov, "A difference method for numerical calculation of discontinuous solutions of the equations of hydrodynamics," *Mat. Sb.* **89**(3), 271–306 (1959).
- ²¹ E. F. Toro, *Riemann Solvers and Numerical Methods for Fluid Dynamics* (Springer, Berlin, 1997).
- ²² S. L. Gavrilyuk, N. Favrie, and R. Saurel, "Modelling wave dynamics of compressible elastic materials," *J. Comput. Phys.* **227**(5), 2941–2969 (2008).
- ²³ S. Ergun, "Fluid flow through packed columns," *Chem. Eng. Prog.* **48**, 89–94 (1952).
- ²⁴ R. R. Bernecker and D. Price, "Studies in the transition to detonation in granular explosives," *Combust. Flame* **22**, 111–129 (1974).
- ²⁵ J. Massoni, R. Saurel, G. Baudin, and G. Demol, "A mechanistic model for shock initiation of solid explosives," *Phys. Fluids* **11**(3), 710–736 (1999).
- ²⁶ R. Saurel, F. Petitpas, and R. Abgrall, "Modeling phase transition in metastable liquids. Application to flashing and cavitating flows," *J. Fluid Mech.* **607**, 313–350 (2008).
- ²⁷ J. Kang, P. B. Butler, and M. R. Baer, "A thermomechanical analysis of hot spot formation in condensed-phase, energetic materials," *Combust. Flame* **89**(2), 117–139 (1992).